Atmos. Chem. Phys. Discuss., 13, 7871–7929, 2013
www.atmos-chem-phys-discuss.net/13/7871/2013/
doi:10.5194/acpd-13-7871-2013

Atmospheric Chemistry and Physics Discussions
Open Access

Key chemical NO_x sink uncertainties and how they influence top-down emissions of nitrogen oxides

T. Stavrakou[1], J.-F. Müller[1], K. F. Boersma[2,3], R. J. van der A[2], J. Kurokawa[4], T. Ohara[5], and Q. Zhang[6]

[1]Belgian Institute for Space Aeronomy, Avenue Circulaire 3, 1180, Brussels, Belgium
[2]Royal Netherlands Meteorological Institute (KNMI), Wilhelminalaan 10, De Bilt, the Netherlands
[3]Eindhoven University of Technology, Fluid Dynamics Lab, Eindhoven, the Netherlands
[4]Asia Center for Air Pollution Research, Niigata, Japan
[5]National Institute for Environmental Studies, Tsukuba, Ibaraki, Japan
[6]Center for Earth System Science, Tsinghua University, Beijing, China

Received: 12 March 2013 – Accepted: 17 March 2013 – Published: 22 March 2013

Correspondence to: T. Stavrakou (jenny@aeronomie.be)

Published by Copernicus Publications on behalf of the European Geosciences Union.

Abstract

Triggered by recent developments from laboratory and field studies regarding major NO_x sink pathways in the troposphere, this study evaluates the influence of chemical uncertainties in NO_x sinks for global NO_x distributions calculated by the IMAGESv2 chemistry-transport model, and quantifies their significance for top-down NO_x emission estimates. Our study focuses on four key chemical parameters believed to be of primary importance, more specifically, the rate of the reaction of NO_2 with OH radicals, the newly-identified HNO_3-forming channel in the reaction of NO with HO_2, the reactive uptake of N_2O_5 on aerosols, and the regeneration of OH in the oxidation of isoprene. Sensitivity simulations are performed to estimate the impact of each source of uncertainty. The model calculations show that, although the NO_2 + OH reaction is the largest NO_x sink globally accounting for 50–70 % of the total sink, the reaction contributing the most to the overall uncertainty is the formation of HNO_3 in NO + HO_2, leading to NO_x column changes reaching a factor of two over tropical regions, and to a 35 % decrease in the global tropospheric NO_x lifetime.

Emission inversion experiments are carried out using model settings which either miminize (MINLOSS) or maximize (MAXLOSS) the total NO_x sink, both constrained by one year of OMI NO_2 column data from the DOMINO v2 KNMI algorithm. The choice of the model setup is found to have a major impact on the top-down flux estimates, with 50 % higher emissions for MAXLOSS compared to the MINLOSS inversion globally. Even larger departures are found for soil NO (factor of 2) and lightning (70 %), whereas the global anthropogenic source is comparatively better constrained, especially in China.

Evaluation of the emission optimization is performed against independent satellite observations from the SCIAMACHY sensor, airborne NO_2 measurements, observed NO_x lifetimes at megacities, as well as with two new bottom-up inventories of anthropogenic emissions in Asia (REASv2) and China (MEIC). Neither the MINLOSS nor the MAXLOSS setup succeeds in providing the best possible match with all independent

ACPD
13, 7871–7929, 2013

datasets. Whereas the minimum sink assumption leads to better agreement with aircraft NO_2 profile measurements, comforting the results of a previous analysis (Henderson et al., 2012), the same assumption leads to unrealistic features in the inferred distribution of emissions over China. Clearly, although our study addresses an important issue which was largely overlooked in previous inversion exercises, and demonstrates the strong influence of NO_x loss uncertainties on top-down emission fluxes, additional processes need to be considered which could also influence the inferred source.

1 Introduction

Sources of nitrogen oxides in the atmosphere are predominantly anthropogenic. According to state-of-art estimates, anthropogenic NO_x accounts for about 65 % of the annual global NO_x flux, whereas natural emissions from fires, soils and lightning are less significant on the global scale, and are estimated at 9 %, 17 % and 6 %, respectively (e.g. Jaeglé et al., 2005; Müller and Stavrakou, 2005). The uncertainties in these estimates are, however, significant, especially for natural sources. To narrow down these uncertainties, top-down or inverse modelling methods constrained by tropospheric NO_2 vertical column abundances observed from space have been widely used to evaluate and complement the bottom-up inventories used in atmospheric models (e.g. Müller and Stavrakou, 2005; Stavrakou et al., 2008; Zhao and Wang, 2009; Lin et al., 2010; Lin, 2012b; Mijling and van der A, 2012; Miyazaki et al., 2012a).

Inverse modelling adjusts the emission fluxes used in a chemistry-transport model in order to reduce the mismatch between the predictions of the model and atmospheric observations. This is often realized iteratively by varying the emissions until the model/data biases are minimized within their assigned errors. This approach implicitly assumes that the relationship between the emission fluxes and the atmospheric abundances is reasonably well simulated by the model, so that the model/data mismatch can be mostly attributed to errors in the emission inventories. In other words, the uncertainties associated to the bottom-up emissions are assumed to be larger

ACPD
13, 7871–7929, 2013

than errors in the model or in the measurements used to constrain the inversion. Nevertheless, a series of recent developments regarding the chemical NO_x sinks, and the chemistry of volatile organic compounds (Mollner et al., 2010; Butkovskaya et al., 2007, 2009; Henderson et al., 2012; Brown et al., 2009; Lelieveld et al., 2008) point to flaws in the current mechanisms implemented in global models, implying potentially large impacts on simulated NO_x concentrations, and consequently on top-down NO_x emission estimates.

These developments concern firstly the main tropospheric NO_x removal channel, i.e. the reaction of NO_2 with OH radicals, forming nitric acid. It was shown in a laboratory study that its reaction rate at room temperature is lower than previously recommended (Mollner et al., 2010), and further, aircraft observations were used to show that its reaction rate in the upper troposphere was even more largely overpredicted at the low temperatures typical of the upper troposphere (Henderson et al., 2012). Secondly, a series of laboratory experiments performed by Butkovskaya et al. (2007, 2009) suggested an additional loss process for NO_x through a nitric acid formation channel in the $NO + HO_2$ reaction. Although this channel is quite minor compared to the traditional pathway forming $NO_2 + OH$ (less than 0.5 % in dry air), it has the potential to represent a significant HNO_3 formation pathway (Cariolle et al., 2008); furthermore, it was found to proceed much faster in the presence of water vapor. This could strongly affect the NO_2 concentrations, especially in the lower troposphere and in tropical regions. Thirdly, field measurements (Brown et al., 2009) suggested that reactive uptake of N_2O_5 at the surface of aerosols proceeds at rates substantially lower than predicted by pameterizations widely used in global models (e.g. Evans and Jacob, 2005; Davis et al., 2008). Finally, there is conclusive evidence that global models strongly underpredict OH radical concentrations, in low-NO_x, high-isoprene environments (Lelieveld et al., 2008; Hofzumahaus et al., 2009). Although the reaction mechanisms responsible for this discrepancy are currently the topic of intense research (Peeters et al., 2009; Crounse et al., 2011; Berndt, 2012), simple expedients have been proposed to crudely compensate for the model underprediction (Lelieveld et al., 2008). A thorough

ACPD
13, 7871–7929, 2013

discussion of the above sources of uncertainty in NO_x concentrations is presented in Sect. 2, and their importance on the NO_2 abundances simulated with the IMAGESv2 global CTM is addressed in Sect. 4.

Based on the above, two model setups are designed to either minimize (MINLOSS simulation) or maximize (MAXLOSS) the NO_x sink in the model. These scenarios are meant to provide a measure of the "state-of-science" uncertainty related to the major chemical NO_x losses. They do not address other sources of uncertainty, however, such as errors related to meteorological fields or other model parameters. Recently, a systematic analysis of meteorological and chemical parameters affecting the NO_x simulation in a CTM by Lin et al. (2012a), showed that errors in meteorology affect only moderately the modelled NO_2 columns, whereas the overall reported uncertainty accounting for all parameters was lower than 20 %.

The MINLOSS and MAXLOSS setups are used in an inverse modelling framework using the adjoint of the IMAGESv2 model (e.g. Müller and Stavrakou, 2005; Stavrakou et al., 2008, 2012). The inversion experiments are constrained by vertical NO_2 tropospheric columns retrieved from the Ozone Monitoring Instrument (OMI) (Boersma et al., 2011) (Sect. 3). The top-down estimates of NO_x fluxes as derived from MINLOSS and MAXLOSS inversions are compared in Sect. 5. Evaluation of the results against independent measurements and inventories is presented in Sect. 6. More specifically, the model predictions before and after inversion are compared against (i) NO_2 column data from SCIAMACHY instrument aboard ENVISAT (Sect. 6.1), (ii) airborne NO_2 profiles from INTEX-A and INTEX-B missions (Sect. 6.2), and (iii) observed NO_x lifetimes in selected megacities (Sect. 6.3). The top-down emissions are also directly compared with two state-of-art bottom-up emission inventories for Asia and for China (Sect. 6.4). Finally, conclusions are drawn in Sect. 7.

ACPD
13, 7871–7929, 2013

2 Uncertainties in NO_x sinks

2.1 The $NO_2 + OH \rightarrow HNO_3$ reaction

Despite its crucial role as the primary sink of NO_x in the troposphere, the rate constant for the termolecular association reaction, $NO_2 + OH + M \rightarrow HNO_3 + M$, has remained very difficult to measure with accuracy under atmospheric conditions. Recently, its expression has been revised by Mollner et al. (2010) based on room temperature experiments performed using improved experimental methods relying on the simultaneous measurement of all reactants and products in the reaction (Donahue, 2011). The measured rates at 298 K were significantly lower than in previous recommendations, by 23 % compared to IUPAC-2004 (Atkinson et al., 2004) and by 13 % compared to JPL (Sander et al., 2011). Since the temperature dependence of the rate was not investigated by Mollner et al. (2010), the recommendation of Sander et al. (2011) is adopted to extrapolate the experimental result of Mollner et al. (2010) at all temperatures, resulting in the following expressions for the low- and high-pressure limits of the reaction: $k_0 = 1.48 \times 10^{-30} \times (T/300)^{-3}\ cm^6\ molecule^{-2}\ s^{-1}$, and $k_{inf} = 2.58 \times 10^{-11}\ cm^3\ molecule^{-1}\ s^{-1}$.

Using upper tropospheric airborne measurements of NO_2, HNO_3, O_3, OH, and HO_2 from the Intercontinental Chemical Transport Experiment – North America (INTEX-NA) in a Bayesian modelling framework designed to constrain reaction rates, Henderson et al. (2012) found that the HNO_3 formation rate in the upper troposphere is overestimated by 22 % when adopting the rate recommendation of Sander et al. (2011). Assuming the experimental rate at 298 K by Mollner et al. (2010) to be correct, Henderson et al. (2012) deduced an updated temperature dependency: $k_0 = 1.48 \times 10^{-30} \times (T/300)^{-1.8}\ cm^6\ molecule^{-2}\ s^{-1}$.

The altitude dependence of the rate calculated using four different recommendations is displayed in Fig. 1 for mid-latitude summer conditions (left panel). Note that the IUPAC rate is overestimated in part because it represents the total $NO_2 + OH + M$ rate

ACPD
13, 7871–7929, 2013

constant, including the minor channel leading to pernitrous acid, HOONO. The latter channel cannot be considered a true NO_x sink, because HOONO rapidly decomposes back to NO_2 and OH in lower tropospheric conditions (Sander et al., 2011). A reasonable estimation for the uncertainty on the nitric acid-forming channel in NO_2 + OH is the difference between the expressions provided by JPL and Henderson et al. (2012). The impact of this uncertainty is explored through three CTM simulations carried out following either Sander et al. (2011), Mollner et al. (2010) or Henderson et al. (2012) (JPL, MOLLNER and MINLOSS, cf. Table 1).

2.2 The NO + HO_2 → HNO_3 reaction

A potentially important NO_x loss process is the minor HNO_3-forming channel in the reaction of NO + HO_2 identified through laboratory observations by Butkovskaya et al. (2005). Its branching ratio, determined experimentally between 223–300 K under dry conditions, was found to strongly vary with temperature (e.g. from 0.18 % at 298 K to 0.87 % at 223 K at 200 Torr), according to the expression

$$\beta_d = 5.3/T + 6.4 \times 10^{-6} P - 0.0173$$

(P in Torr) (Butkovskaya et al., 2005, 2007; Cariolle et al., 2008).

The overall reaction rate under dry conditions (k_d) is the product of this branching ratio by the Sander et al. (2011) recommended value for the NO + HO_2 reaction rate:

$$k_d = 3.3 \times 10^{-12} \exp(270/T) \times \beta_d .$$

Recent modelling studies have investigated the impacts of the addition of the new channel on the distribution of HNO_3, NO_x, HO_x and O_3 (Cariolle et al., 2008) and on the trends of atmospheric species and radiative forcing (Søvde et al., 2011).

Further experiments showed that the HNO_3 yield is strongly enhanced in presence of water vapour (Butkovskaya et al., 2009). Assuming that this effect is due to the reaction of NO with the $HO_2 \cdot H_2O$ complex, the rate of the reaction NO + $HO_2 \cdot H_2O$ → HNO_3 was

ACPD
13, 7871–7929, 2013

estimated at room temperature:

$$k_w = 6 \times 10^{-13}\,\mathrm{cm^3\,molecule^{-1}\,s^{-1}}.$$

Since the effect of water was investigated only at 298 K, this rate is assumed here to be temperature-independent. The complexed fraction f_c of the hydroperoxyl radical HO_2 is estimated from the equilibrium constant of $HO_2 + H_2O \leftrightarrow HO_2{\cdot}H_2O$:

$$f_c = \frac{1}{1 + 1/(K_{eq} \times [H_2O])},$$

with $K_{eq} = 1.57 \times 10^{-24} \exp(3775/T)\,\mathrm{cm^3\,molecule^{-1}}$. This expression for K_{eq} is based on its measured value at 297 K, $5.2 \times 10^{-19}\,\mathrm{cm^3\,molecule^{-1}}$ (Kanno et al., 2005), and on an enthalpy of $\Delta H = 7.5\,\mathrm{kcal\,mol^{-1}}$, close to the value of $7.42\,\mathrm{kcal\,mol^{-1}}$ reported in the theoretical study of Alongi et al. (2006). The overall rate of the $NO + HO_2 \rightarrow HNO_3$ reaction in moist air can then be estimated using

$$k = k_d \times (1 - f_c) + k_w \times f_c.$$

The H_2O-assistance in the HNO_3-forming channel leads to a factor of 2–3 increase of the rate constant below 4 km (Fig.1, middle panel), whereas the gap closes at higher altitudes as air becomes drier. The temperature dependence of k_w adds therefore little uncertainty to the overall impact of this reaction in the troposphere, since low temperature is generally associated with dry air. The implications of the new reaction on the global modelled NO_2 columns are investigated in two simulations, with and without accounting for the effect of H_2O-assistance (BUTKO1, BUTKO2, Table 1).

2.3 Heterogeneous reaction on sulfate aerosols

The heterogeneous hydrolysis of N_2O_5 at the surface of aerosols is an important NO_x loss process during nighttime. Its overall impact is largest in polluted environments

ACPD
13, 7871–7929, 2013

(where aerosol loadings and N_2O_5 formation rates are high) during winter (when nights are longer and hydroxyl radical levels are at their lowest). Among different aerosol types, sulfate-containing aerosols are putatively characterized by the highest reaction probability (e.g. Evans and Jacob, 2005). Two commonly used parameterizations for the reaction probability on sulfate-containing aerosols ($\gamma_{N_2O_5}$) by Evans and Jacob (2005) and by Davis et al. (2008), are based on laboratory measurements and account for the effect of temperature and relative humidity. Davis et al. (2008) provide a further distinction between different sulfate- and nitrate-containing aerosols, including sulfuric acid, ammonium sulfate, bisulfate and nitrate. Evans and Jacob (2005) also propose recommendations for the reaction probability on organic and black carbon, dust and sea-salt. The possible influence of organics on $\gamma_{N_2O_5}$ is, however, neglected in both parameterizations.

Brown et al. (2009) determined reactive uptake coefficients for N_2O_5 using field measurements of O_3, NO_x, and aerosol surface area obtained during the night flights of the TexAQS II (Second Texas Air Quality Study) campaign in 2006. This study revealed that $\gamma_{N_2O_5}$ (i) lies in the range $0.5–6 \times 10^{-3}$, i.e. much lower than previously reported laboratory-based values, and (ii) contrary to current belief, does not exhibit a clear dependence on relative humidity or aerosol composition. The average value for the uptake coefficient derived by these measurements is equal to 0.003, by up to an order of magnitude lower than in parameterizations currently utilized in atmospheric models. Supporting evidence for the low value of the uptake coefficient is provided by direct N_2O_5 reactivity measurements on ambient aerosol particles (Bertram et al., 2009), where the observed values were found to be by a factor of ten lower compared with current parameterizations. Organic material at the aerosol surface has been identified as a candidate explanation for the reduction of the accomodation coefficient (McNeill et al., 2006).

The N_2O_5 sink rate on sulfates calculated for mid-latitude winter conditions using different parameterizations are compared in Fig. 1 (right panel). Overall, the Brown et al. (2009) value leads to a sink lower by a factor of 2–3 compared to the Davis et al.

ACPD
13, 7871–7929, 2013

(2008) parameterization, and a factor of 2–8 compared to Evans and Jacob (2005). To evaluate the impact of these differences on the NO_x budget and distribution, we contrast the results of two simulations, one using a constant value of 0.003 for the uptake coefficient, as suggested by Brown et al. (2009), and one using the Davis et al. (2008) parameterization (MINLOSS and DAVIS simulations, respectively).

2.4 Other losses

In addition to the previous pathways of NO_x removal, the following processes are also considered.

- Dry deposition of NO_2. The dry deposition of NO_2 to vegetation and soils is a direct NO_x sink, computed with the resistance-in-series scheme of Wesely (1989).

- Wet and dry deposition of organic nitrates. NO_x is converted to organic nitrate through reactions of NO_3 with alkenes, as well as through reactions of peroxy radicals with NO and acyl peroxy radicals with NO_2. Organic nitrates are temporary NO_x reservoirs with lifetimes of the order of minutes to weeks which can be transported away from the source regions, where they can either release NO_2 through decomposition or oxidation, or undergo wet and/or dry deposition. Besides peroxy acyl nitrates (PANs), isoprene nitrates are believed to represent the largest contribution to the total organic nitrate budget (Beaver et al., 2012; Browne and Cohen, 2012), although their precise yields and fate remain poorly understood. Their role is relatively limited in IMAGESv2 due to their short lifetimes, and to the simplifying assumption that their reaction with OH releases NO_2, as in the MIM2 mechanism (Taraborrelli et al., 2009). In itself, nitrate formation and export should not be considered a NO_x sink, although it might significantly deplete NO_x levels in the formation region (Paulot et al., 2012). In this section, only the deposition of organic nitrate will be considered a NO_x sink. However, when evaluating the modelled NO_x lifetimes against measurement-based estimations at a local level (e.g.

ACPD
13, 7871–7929, 2013

a megacity), the net organic nitrate formation rate should be taken into account (see Sect. 6.3).

– Reaction of NO_3 with aldehydes and with dimethylsulfide $(CH_3)_2S$. NO_3 can be converted to nitric acid by reaction with aldehydes, $NO_3 + RCHO \rightarrow HNO_3 + RCO^{\bullet}$, or by reaction with dimethylsulfide, $NO_3 + (CH_3)_2S \rightarrow HNO_3 + CH_3SCH_2$. Whereas the reaction with aldehydes is found to be almost negligible in our model calculations, the reaction with $(CH_3)_2S$ is significant above oceans.

According to our model calculations, the sum of the above sinks represents only a small part (ca. 18 %) of the global tropospheric NO_x sink (Table 1). Uncertainties related to these sinks will not be addressed in this study, although they might be substantial. As a result, the overall NO_x sink uncertainty derived in this study should only be seen as a lower limit. In particular, a more detailed treatment of organic nitrate chemistry could result in increased NO_x sinks in regions influenced by biogenic isoprene emissions.

2.5 OH radical concentration

An additional source of uncertainty resides in the abundances of OH radicals, responsible for the conversion of NO_2 to nitric acid as well as for the removal of most reactive compounds in the troposphere. We discuss briefly below three possibly major reasons for this uncertainty, namely, the degradation chemistry of isoprene, the production of HONO, whose photolysis provides a direct OH source, and the heterogeneous HO_2 loss on aerosols.

There is strong evidence from field campaigns in mid-latitude forests, tropical forests and other rural environments (e.g. Lelieveld et al., 2008; Ren et al., 2008; Hofzumahaus et al., 2009) that OH levels are largely underestimated in models when using traditional isoprene chemical chemistry (Butler et al., 2008; Kubistin et al., 2010; Stone et al., 2011). Furthermore, the model underprediction is found to increase for increasing isoprene concentrations as well as for decreasing NO levels (Lu et al., 2013). Although

ACPD
13, 7871–7929, 2013

the causes of this behaviour are still under heated debate, they imply the existence of OH recycling processes counteracting the OH suppression due to reaction with isoprene and its degradation products. Lelieveld et al. (2008) suggested that between 2 and 4 OH radicals are formed in the reaction of isoprene peroxy radicals with HO_2 as implemented in the MIM2 chemical mechanism (Taraborrelli et al., 2009). Although this approach allowed to better align the model to the data, it was not supported by theoretical or experimental evidence. A substantial progress towards the elucidation of the high observed OH concentrations was provided by the theoretical studies of Peeters et al. (2009) and Peeters and Müller (2010), proposing that the isomerization of specific isoprene peroxy radicals leads to substantial HO_x regeneration. Tested in global models (e.g. Stavrakou et al., 2010), the mechanism was found to be very efficient in enhancing HO_x concentrations in the boundary layer, providing good agreement with available data. However, several open issues merit further investigation, e.g. the subsequent degradation chemistry of the isomerization products, as well as the reconciliation of theoretical findings with experimental evidence from the laboratory (Crounse et al., 2011).

The second source of uncertainty in OH levels originates in the primary OH radical source through HONO photolysis, which has been identified from field observations as quite significant in the lower troposphere, especially in the early morning (e.g. Elshorbany et al., 2009). A strong missing source of HONO has been invoked by recent studies to reconcile the large discrepancies found between observed and modelled HONO abundances during daytime (Sörgel et al., 2011; Su et al., 2011). The formation processes leading to these unexpectedly enhanced HONO concentrations are still under investigation, like nitrate photolysis following HNO_3 deposition on forest canopy surfaces (Zhou et al., 2011), heterogeneous conversion of NO_2 on ground and aerosol surfaces (Su et al., 2008), or HONO release from soil nitrites (Su et al., 2011). However, evidence favoring one or the other process is still partial, and therefore, the atmospheric impact of HONO, in particular its contribution to the production of OH radicals, remains an open issue.

ACPD
13, 7871–7929, 2013

Finally, the reactive uptake of HO_2 by aerosols is a potentially important yet very uncertain HO_x sink. A reaction probability (γ_{HO_2}) value of 0.2 has been recommended for use in atmospheric models (Jacob, 2000), and is adopted in the baseline model simulation (MINLOSS). Laboratory measurements at atmospherically-relevant conditions revealed that the uptake coefficients for dry $(NH_4)_2SO_4$ and NaCl aerosol were lower than 0.05, whereas for wet aerosols, measured γ_{HO_2} ranged between ca. 0.1 and 0.2 (Taketani et al., 2008). On the other hand, values higher than 0.2 have been observed in the presence of transition metal ions in aqueous aerosols (Cooper and Abbatt, 1996; Taketani et al., 2008). Based on a compilation of available measurement data, the parameterization of Macintyre and Evans (2011) for the uptake coefficient of HO_2 on sulfates, black and organic carbon, sea salt and dust suggests a global mean value of 0.028, the uptake being more significant on sulfates (up to 0.3). Over polluted areas, the uptake on sulfates is the dominant component of the total aerosol sink, and therefore, only this component is considered in our study.

In order to test the uncertainties related to isoprene chemistry, we performed a sensitivity simulation denoted MIM2+ (Table 1), which includes the recycling mechanism proposed by Lelieveld et al. (2008). The OH production from HONO is not considered in the current version of the model. We test the sensitivity of the model with respect to uncertainties in HO_2 aerosol uptake by carrying out a simulation where γ_{HO_2} is set to a lower value, equal to 0.05 (HO2L run of Table 1).

3 Satellite-driven source inversion of NO_x sources

3.1 Tropospheric NO_2 columns from OMI

OMI (Ozone Monitoring Instrument) is a Dutch–Finnish nadir viewing imaging spectrometer flying on a sun-synchronous orbit crossing the local equator at ca. 13:40 LT (Levelt et al., 2006). Launched aboard the Aura platform in 2004, OMI measures in the UV-visible spectral window (270–500 nm) at a nadir resolution of 13 × 24 km. The Dutch

ACPD
13, 7871–7929, 2013

OMI tropospheric NO_2 version 2 (DOMINO v2) data product (Boersma et al., 2011), publicly available through the TEMIS portal (http://www.temis.nl), is used in this study. This version constitutes a major improvement compared to the previous DOMINO v1 tropospheric NO_2 columns (Boersma et al., 2011). DOMINO v2 has been used thus far in assimilation studies (Miyazaki et al., 2012a,b), air quality assessments (McLinden et al., 2012), as well as for validation purposes (Irie et al., 2012; Ma et al., 2013).

DOMINO v2 tropospheric NO_2 columns are reduced by 20 % in winter, and by 10 % in summer over polluted regions, compared to the DOMINO v1 product. Larger discrepancies between DOMINO v2 and v1 occur, however, on regional scales. The OMI tropospheric NO_2 retrieval error for individual, cloud-free pixels comprises the uncertainties on the slant and on the stratospheric slant column, estimated at 0.7×10^{15} and 0.15×10^{15} molec cm^{-2}, respectively, and the uncertainty on the tropospheric AMF, lying between 10 and 40 % (Boersma et al., 2007). The total error of the DOMINO v2 product is estimated to be lower, from 1.0×10^{15} molec cm^{-2} + 30 % for v1, to 1.0×10^{15} molec cm^{-2} + 25 % for DOMINO v2 (Boersma et al., 2011).

3.2 NO_2 simulated by IMAGESv2 CTM

The IMAGESv2 global chemistry-transport model simulates the concentrations of 132 trace species at a resolution of $2^\circ \times 2.5^\circ$, and at 40 sigma-pressure levels between the Earth's surface and the lower stratosphere (44 hPa). Meteorology is obtained from ERA-Interim analyses of the European Center of Medium-Range Weather Forecasts (ECMWF) for the year of the simulation (2007). Details about the model can be found in previously published work (Müller and Stavrakou, 2005; Stavrakou et al., 2008). The chemistry is solved by the fourth order Rosenbrock solver of the Kinetic Preprocessor software tool (KPP, Sandu et al., 2006). The model time step for the forward simulations is taken equal to 4 h. The effects of diurnal variations are accounted for through correction factors calculated from a detailed model run with a 20 min time step, which is also used to estimate the NO_2 column diurnal shape profile. This diurnal cycle simulation

ACPD
13, 7871–7929, 2013

accounts for diurnal variations in the photolysis and kinetic rates, in the meteorological fields, and in the emissions.

The model uses anthropogenic emissions from the EDGAR 3.2 FT2000 inventory for year 2000 (http://themasites.pbl.nl/tridion/en/themasites/edgar/), overwritten by the REAS (Ohara et al., 2007) inventory over Asia, and EMEP emissions over Europe (http://www.ceip.at/). Over the US, the EDGAR emission is scaled to the National Emission Inventory (NEI, http://www.epa.gov/ttn/chief/eiinformation.html) values for each year.

The seasonality of anthropogenic emissions accounts for (i) a temperature dependence of vehicle emissions from the MOBILE 6 algorithm (Giannelli et al., 2002), and (ii) the seasonal variation of residential heating. In MOBILE 6, the effect of cold starts on CO road transport emissions is accounted for by a correction factor applied for temperatures lower than 18 °C, equal to $1 + (18 - T_C) \times 0.05$, with T_C the temperature in Celsius. Road emissions of NO_x are only slightly temperature-dependent, a correction factor equal to $1 + (24 - T_C) \times 0.0072$ being applied only for temperatures above 24 °C. The sectoral split of anthropogenic emissions is obtained from EDGAR. The seasonal variation of heating emissions is estimated by assuming that these emissions are proportional to the number of heating degree-days, with a threshold of 18 °C.

Diurnal and weekly profiles of CO, NO_x and VOC anthropogenic emissions for OECD countires are obtained from Jenkin et al. (2000). A diurnal cycle is also applied to biomass burning emissions (Stavrakou et al., 2009a) as well as to lightning emissions, assumed to follow the diurnal cycle of convective updraft fluxes.

For the year 2007, global annual anthropogenic NO_x emissions (excluding ship and aircraft emissions) are estimated at 25.7 Tg N. Emissions from ships and aircraft contribute to an additional 4.2 Tg N in 2007. Open vegetation fires are obtained from the Global Fire Emission Database (GFEDv3, van der Werf et al., 2010) and amount to 4.3 Tg N globally in 2007. The horizontal distribution of lightning NO emissions (scaled at 3 Tg N yr^{-1} globally) combines a spaceborne climatology (LIS/OTD) for the number of flashes with a parameterization (Price and Rind, 1993; Martin et al., 2007) which uses cloud top heights and convective precipitation rates from ECMWF. The lightning

ACPD
13, 7871–7929, 2013

emissions are vertically distributed according to Pickering et al. (1998). Emissions of organic and black carbon aerosols are taken from Bond et al. (2004) and van der Werf et al. (2010). Inorganic aerosols are calculated by EQSAM (Metzger et al., 2002). The wet removal scheme for gases and aerosols is described in Stavrakou et al. (2009c).

Soil emissions are calculated according to the algorithm of Yienger and Levy (1995). Biome data are taken from the compilation of Matthews (1983) (http://data.giss.nasa.gov/landuse/vegeem.html), and cropland distribution from the land use database of Klagenfurt University (Erb et al., 2007). Total fertiliser consumption per year and per country is obtained from the International Fertiliser Association (IFA, http://www.fertilizer.org), and the fraction of fertiliser consumption which is used in rice paddies is obtained from the Food and Agriculture Organization (FAO, http://faostat.fao.org). The fraction of the applied fertilizer assumed to be lost as NO is equal to 1 % for all crops (Steinkamp and Lawrence, 2011), except for rice paddies where it is assumed to be zero (Yienger and Levy, 1995). The total soil emission is scaled to 8 Tg N globally.

Nine forward global simulations are performed (Table 1) to evaluate the sensitivity of the calculated NO_2 column and NO_x lifetime to the NO_x sink uncertainties described in Sect. 2. The simulations are performed for year 2007, and the model is initialized on 1 September 2006. (cf. Sect. 3.3).

The simulated monthly averaged NO_2 columns are compared to the corresponding DOMINO v2 averages binned at the horizontal resolution of the model, while accounting for the instrument averaging kernels and for the sampling times of observation at each location. The errors associated to the monthly DOMINO v2 averages are estimated from the reported retrieval errors, following a super-observation approach as in Miyazaki et al. (2012a), and accounting for an assumed error correlation of 50 % between retrieval errors on individual measurements contributing to the same super-observation. The total monthly error combines this super-observation retrieval error and an assumed model/representativity error of 0.5×10^{15} molec cm^{-2}.

ACPD
13, 7871–7929, 2013

3.3 The inversion setup

The discrete adjoint of the IMAGESv2 model is used to infer top-down NO_x emission estimates constrained by OMI columns. This method, described in previous work (Stavrakou et al., 2006, 2008), allows for deriving monthly emission estimates at the resolution of the model ($2^\circ \times 2.5^\circ$) for each of the NO_x emitting categories (anthropogenic, biomass burning, soil and lightning). The assumed error on the anthropogenic emissions by country is set equal to a factor of 1.6 and 2 for OECD and other countries, respectively, to a factor of 2 for soil emissions, and 2.5 for vegetation burning and lightning.

Two optimizations are carried out, which use NO_x sink assumptions of either the MINLOSS and MAXLOSS simulations (Table 1). They are performed at $2^\circ \times 2.5^\circ$ model resolution and use one year (2007) of OMI NO_2 global columns as constraints. The total number of control variables to be optimized in these source inversions is approximately equal to 70 000.

4 Importance of uncertainties of NO_x losses addressed with IMAGESv2

Using MINLOSS as our baseline run, the influence of the chemical uncertainties discussed in Sect. 2 is illustrated by their impact on the sink rate of the tropospheric NO_x column in January and July (Figs. 2 and 3). By far the largest impact is the change due to the HNO_3 forming channel in the reaction $NO + HO_2$, especially when H_2O-assistance is included (BUTKO1-2). The impact reaches up to a factor of two over tropical oceans, as a result of the high abundance in HO_2 and water vapour in these regions (Fig. 2d). Over polluted regions, the relative impact of this loss process is found to be lower, although it remains still significant, especially in summer (up to 25 %). Overall, the relative contribution of this reaction to the global tropospheric NO_x sink amounts to 14 % in the case of BUTKO1 scenario, and reaches 27 % when water-assistance is taken into account. As a result, the global NO_x lifetime is reduced by 18 % and 26 %

ACPD
13, 7871–7929, 2013

in BUTKO1 and BUTKO2, respectively, compared to the base run. Including this reaction channel results in an overall decrease of NO_x columns by up to 45 % (60 %) at remote oceanic regions, and by 15 % (30 %) over the continental Tropics in BUTKO1 (BUTKO2) cases, whereas the decrease over polluted continental regions is much less important (ca. 5 % in the US). As expected, the impact of the additional sink is largest for chemically aged air masses, far away from the emission regions. For the same reason, calculated changes in the surface NO_2 mixing ratios generally do not exceed 15 % over continents, even in the BUTKO2 simulation. As an effect of the lower NO_x abundances, O_3 production is reduced by 4–6 % in the mid-latidudes near the surface, and by up to 16 % at remote environments to the south of 50° S in the BUTKO1 run, in very good agreement with the changes reported by Cariolle et al. (2008). The enhanced NO_x sink in BUTKO2 run leads to more pronounced decreases of model surface O_3, by 7–10 % in mid-latitudes and by 24 % at latitudes south of 50° S.

The replacement of the low constant value for $\gamma_{N_2O_5}$ (0.003) by the Davis et al. (2008) parameterization for the uptake of N_2O_5 on aerosols in the DAVIS simulation leads to substantial increases in the loss rate of the NO_x column in the northern extratropical latitudes during winter. This is attributed to the low HO_x levels at this time of the year, to the presence of high NO_x and aerosol sources in these regions, and to the strong dependence of the Davis et al. (2008) parameterization on relative humidity. The enhancement of the sink rate reaches 100 % in these regions in January. In July, the importance of this reaction is drastically reduced due to the dominance of the $NO_2 + OH$ sink (Figs. 2, 3e). The sensitivity is weak in the Tropics. Globally, this sink, which accounts for 8 % of the global sink in the baseline simulation, is almost doubled in the DAVIS case, and is responsible for a reduction of the global NO_x lifetime by 6 % (Table 1). The parameterization by Davis et al. (2008) results in NO_x column decreases reaching 30 % at high latitudes in wintertime, although these changes are more limited over emission regions.

The reaction of NO_2 with OH constitutes the major loss of NO_x in the troposphere, estimated to represent more than 70 % of the total NO_x sink globally. The sensitivity

ACPD
13, 7871–7929, 2013

of this sink with respect to the use of the Mollner et al. (2010) rate constant instead of the Henderson et al. (2012) expression is found to be weak in both seasons, generally of the order of 10 %, except at remote southern latitudes where it reaches 20 % (MOLLNER, Table 1, Figs. 2a, 3a). This can be explained by the stronger temperature dependence assumed in the MOLLNER case (Fig. 1) compared to MINLOSS, which reinforces the NO_x loss in the upper troposphere, especially away from NO_x sources, because at these regions the relative contribution of this sink at the surface is minor. In the JPL run, more pronounced increases in the NO_x loss rate are found, reaching 30 % over the remote regions of the Southern Hemisphere. Globally, the calculated NO_x lifetime is found to decrease by 6 % and 12 % in the MOLLNER and JPL simulation, respectively.

The effect of the model changes in the MIM2+ and HO2L simulations is found to be small, or even insignificant. In the MIM2+ simulation, the increased OH concentrations over forested areas lead to increased NO_x loss rates. The sink increase amounts to less than 1 % on the global scale, but can reach 20 % in isoprene-rich regions (Figs. 2f, 3f). Further, the model using the lower reaction probability for the sulfate aerosol uptake of HO_2 (HO2L simulation) exhibits a very small global sensitivity (Table 1), except in regions with high aerosol concentrations (see also Macintyre and Evans, 2011).

As seen from this analysis, the base run MINLOSS realizes the lowest NO_x loss rates and the largest global tropospheric NO_x lifetime among the sensitivity tests. The MAXLOSS scenario is designed by adopting those choices which maximize the NO_x loss. This is realized by using the JPL recommendation for the $NO_2 + OH$ reaction rate, by including the HNO_3 forming channel in $NO + HO_2$, based on Butkovskaya et al. (2009), the uptake probability of N_2O_5 on sulfate aerosols from Davis et al. (2008), and the MIM2+ chemistry. The combination of these settings causes a strong reduction of the global NO_x lifetime, by a factor of 1.6 with respect to MINLOSS (Table 1). Note that other model uncertainties could possibly affect the modelled NO_x columns, e.g. in meteorological parameters, in the emissions of other compounds (e.g. NMVOCs) or in chemical parameters other than those considered in this study (Lin et al., 2012a). The

ACPD
13, 7871–7929, 2013

comparison of our MINLOSS and MAXLOSS simulations should, nevertheless, provide a measure of the uncertainties associated to the major chemical NO_x pathways.

The NO_x lifetimes calculated for MINLOSS and MAXLOSS cases are shown in Fig. 4 and the contribution of the main individual NO_x sinks to the total sink is illustrated in Fig. 5 for MAXLOSS. Lifetimes of less than one day are calculated in the case of MAXLOSS over most continental regions, especially in summertime and in high-NO_x environments, due to the dominance of the loss via OH. In essence, the distribution of the $NO_2 + OH$ sink reflects mainly the boundary layer OH concentration field pattern (Fig. 5). The loss via $NO + HO_2$ occurs mostly over tropical regions, and is, on average, roughly two times lower than the loss due to $NO_2 + OH$. In January, N_2O_5 uptake by aerosols is quite significant in regions with high aerosol concentrations and long nights, and is estimated to be three times more important than in July at the global scale (Fig. 5). Over oceans and high-latitude regions the lifetime can reach several days due to lower OH levels and low NO_2 concentrations.

5 Top-down NO_x emissions

This section focuses on the results of the two emission inversions constrained by 2007 OMI data performed using either the MINLOSS or the MAXLOSS model settings (Table 1). The a priori and optimized tropospheric NO_x budget is summarized in Table 2, and the annual total NO_x emission update is shown in Fig. 6.

The differences between the emissions inferred by both inversions are found to be substantial, with the total NO_x source being 50 % higher in MAXLOSS compared to MINLOSS. The top-down estimates, 44 Tg N from MINLOSS against 66 Tg N from MAXLOSS, correspond to a slight decrease of the source (3 %) in the former case, and a substantial increase by 47 % in the latter, with respect to the a priori source. The annual total NO_x emission update, i.e. the ratio of a posteriori to the a priori emissions (Fig. 6), is found to be lower than one at mid-latitudes in MINLOSS, except over Northeastern China. In tropical regions the emissions are increased by up to a factor

ACPD
13, 7871–7929, 2013

of two, mainly due to increased natural sources. Similar patterns are found in the case of MAXLOSS, but with much higher emission updates, generally between 1 and 2 over polluted regions, and between 2 and 5 in the Tropics.

The largest discrepancies between the two inversions concern natural emissions. Global NO_x emissions from lightning and soil differ between by 70 % and 100 % between MAXLOSS and MINLOSS, respectively. This is the consequence of the large difference in NO_x lifetimes between the two inversions in tropical regions (Fig. 4). This difference is further amplified by chemical feedbacks, because the larger NO_x increases in MAXLOSS lead to higher OH levels, and therefore, to further NO_x lifetime decreases. In comparison to most global inversion studies, soil NO emission is found to be generally underestimated by the algorithm of Yienger and Levy (1995). Top-down studies derived estimates for the global soil NO source ranging between 8.9 Tg N (Jaeglé et al., 2005) and 10–12 Tg N (Müller and Stavrakou, 2005; Stavrakou et al., 2008). More recently, improvements upon the algorithm of Yienger and Levy (1995) resulted in new parameterizations yielding global above-soil NO_x emission of 10.7 Tg N (Hudman et al., 2012), and an above-canopy soil NO_x source at 8.6 Tg N (Steinkamp and Lawrence, 2011), in better agreement with satellite-derived fluxes. In the latter study, which was based on a compilation of a large number (ca. 600) of flux measurements, the emission factors for the different ecosystems were estimated from the geometrically averaged observed fluxes. However, the use of an alternative, equally plausible averaging method (the plain arithmetic average) resulted in an annual estimate of 27.6 Tg N, much higher than all previous values. This finding underscores the high uncertainty of this source, whereas the wide range of our OMI-derived estimates for soil emissions, 8.8–17.9 Tg N per year (Table 2), could be regarded as a top-down uncertainty range for this source.

The global NO_x production from lightning derived in this study is estimated at 3.0–5.2 Tg N yr^{-1}, i.e. 0–70 % higher than the a priori source, with the strongest increases predicted in the Tropics. This result is in line with previously reported top-down values, ranging between 1.1 and 6.4 annually (Müller and Stavrakou, 2005; Stavrakou et al.,

ACPD
13, 7871–7929, 2013

2008; Boersma et al., 2005). Recently, Murray et al. (2012), based on satellite lightning data, estimated a global annual source of 6 ± 0.5 Tg N, in agreement with the best estimate of 6 Tg N by Martin et al. (2007) derived through comparisons of satellite observations of NO_2, O_3 and nitric acid with a global CTM, and with the study by Schumann and Huntrieser (2007) reporting a range of 2–8 Tg N per year, based on a literature review suggesting that a thunderstorm flash produces $15(2–40) \times 10^{25}$ molecules NO per flash on average. However, this result was contradicted by a more recent study (Beirle et al., 2010) using SCIAMACHY NO_2 columns, which suggested that the production efficiency is of the order of 2×10^{25} molecules NO per flash, at the low end of the range derived by Schumann and Huntrieser (2007). Should this be confirmed, the global annual NO production would be of the order of 1 Tg N.

Both inversions suggest that the emissions from fires are higher than estimated by the a priori GFEDv3 vegetation fire inventory. On the global scale, the inferred annual values are larger than the a priori, 5 Tg N in MINLOSS, 7.1 in MAXLOSS compared to 4.3 Tg N in GFEDv3. The strongest emission increments are found over Southern Africa (factor of 2–2.5) and Oceania, whereas fire emissions in South America are very close to the prior. Support for higher NO_x emissions from fires is provided by an independent global database of fire emissions (Fire Inventory from NCAR, Wiedinmyer et al., 2011), where the global 2007 emissions are estimated at 6.7 Tg N.

The differences in anthropogenic global totals inferred by the inversions are significant, 26.7 Tg N in MINLOSS vs. 36.2 Tg N in MAXLOSS (cf. Table 2). Pronounced differences are also derived on the continental scale, as illustrated in Table 2. In Europe and North America the posterior emissions are lower than the a priori in the MINLOSS inversion, but higher when the maximum loss scenario is considered. Exception is made for China for which quite robust estimates are found in both inversions, 5.8 Tg N in MINLOSS vs. 6.5 in MAXLOSS, consistently higher than the a priori. This is close to the 2006 top-down anthropogenic flux estimate derived from SCIAMACHY NO_2 columns, 6.3 Tg N yr^{-1} (Stavrakou et al., 2008), but is lower than reported in a recent inversion study for East China (101.25–126.25° E, 19–46° N), 7.1 Tg N yr^{-1}, also constrained by

ACPD
13, 7871–7929, 2013

DOMINO v2 NO_2 columns (Lin, 2012b). Based on a bottom-up methodology for China, Zhang et al. (2007) estimated the anthropogenic emission in 2004 at 5.7 Tg N yr^{-1}. Extrapolating this value based on the emission growth rate derived by Zhang et al. (2007) between 1995–2004 (6.1 % yr^{-1}) would result in an emission estimate of 6.8 Tg N in 2007, very close to the MAXLOSS result. Two recently available bottom-up inventories, namely, the latest version of the Regional Emission inventory in ASia (REAS version 2) and the Multi-resolution Emission Inventory in China (MEIC) will be compared with the OMI-derived emissions in Sect. 6.4.

The flux estimates for North America and Europe are found to depend strongly on the inversion setup. In North America, they are found to be lower (5 Tg N) or higher (7.2 Tg N) in comparison with the a priori (6 Tg N) in MINLOSS and MAXLOSS, respectively, whereas the previous top-down estimate for the same region in 2006 by Stavrakou et al. (2008) lies within the above range, and is very close to the a priori (6.1 Tg N yr^{-1}). In Europe, based on data assimilation of DOMINO v2 NO_2 columns, Miyazaki et al. (2012a) reported an anthropogenic annual flux equal to 4.6 Tg N, close to our a priori value.

The lower sensitivity of top-down emissions to the NO_x sink rates over China compared to, e.g. Europe, North America and tropical regions is very likely a consequence of the very high NO_x concentrations typically found over Northeastern China. Indeed, the positive response of OH levels to NO_x emissions typically found in most tropospheric conditions becomes weaker and even changes sign at those very high NO_x levels. As a result, emission enhancements over China in the MAXLOSS inversion are not accompanied by larger OH level increases compared to MINLOSS, as opposed to the other regions where the chemical feedbacks tend to amplify the differences between MAXLOSS and MINLOSS emission updates.

One fifth of the NO_x source predicted by MAXLOSS is removed via the $NO + HO_2$ reaction. Owing to this additional channel, the relative contribution of the $NO_2 + OH$ loss to the total sink is weakened in the MAXLOSS case study (~ 50 %) compared to MINLOSS (ca. 74 %). The optimization infers very similar magnitudes for the $NO_2 + OH$

ACPD
13, 7871–7929, 2013

sink in both cases (33 vs. 37 Tg N), whereas the uptake of N_2O_5 on sulfate aerosols is found to increase substantially (more than a factor of 3) in MAXLOSS inversion compared to MINLOSS, due to higher NO_x emissions and the non-linear dependence of N_2O_5 formation on NO_x levels. Note that the NO_x sources are not exactly balanced by the sinks due to the small conversion of HNO_3 to NO_x, mostly via oxidation by OH.

The percentage differences between inferred total NO_x emissions in simulations MINLOSS and MAXLOSS (Fig. 7) are less pronounced at mid-latitudes in January (generally less than 30 %) than in July (40–100 %). This weak sensitivity of winter fluxes is partly explained by the longer NO_x lifetimes (> 1 day), and therefore, the increased role played by transport in determining NO_x columns over emission regions in winter. Furthermore, the winter losses are primarily due to the uptake of N_2O_5 on aerosols (Fig. 5) which, although being very uncertain (Fig. 1), is a process operating at night and having therefore only a modest influence on NO_x columns at the overpass time of OMI (13:40 LT).

Both inversions are found to modify the seasonality of anthropogenic emisssions over China (Fig. 8), improving the agreement with the bottom-up inventory of Zhang et al. (2007). The December-to-July emission ratio, equal to 1.25 in the a priori and in MINLOSS, and equal to 1.13 in MAXLOSS, is very close to the ratio reported in Zhang et al. (2007) (1.26). Further, the inferred seasonality is compared with the bottom-up seasonality from two new emission inventories for China (cf. Sect. 6.4). In North America and Europe, the inversions keep the main seasonality features of the a priori almost unchanged. The February peak of the a priori seasonality, due to the low temperatures and the heating-degree day approach applied to the residential emissions, is consistent with the satellite observations, especially in the MINLOSS inversion.

ACPD
13, 7871–7929, 2013

6 Comparisons with independent observations and inventories

6.1 SCIAMACHY NO_2 vertical columns

We evaluate the modelled a priori and a posteriori NO_2 columns against NO_2 column abundances retrieved from the SCIAMACHY UV-visible nadir sounder crossing the local equator at ca. 10:00 LT. SCIAMACHY has a ground pixel of $30 \times 60\,km^2$ and achieves global coverage within six days. For these comparisons we use SCIAMACHYv2 data distributed via the TEMIS website (www.temis.nl, Boersma et al., 2004). This product is reprocessed using the same basic algorithm for satellite observations used for DOMINO v2. Comparisons above selected regions between modelled NO_2 columns before and after inversion and columns from OMI and SCIAMACHY are illustrated in Figs. 9 and 10.

Overall, the model/OMI data discrepancy is efficiently reduced after the optimization. Whereas relatively small changes are inferred in summer over Northern China, the column increases are more substantial in wintertime (up to factor of two), despite the reduced seasonality of anthropogenic emissions (Fig. 8). As discussed in Stavrakou et al. (2008), different photochemical regimes in summer and in winter lead to different responses of the NO_x lifetime to an emission increase, primarily because OH levels increase with NO_x in summer (due to the $HO_2 + NO$ reaction), resulting in a negative feedback, whereas the opposite effect prevails in winter (due to $OH + NO_2$). The role of N_2O_5 is limited because it operates only at night, as noted above.

The bias between the model and the SCIAMACHY data is significantly reduced in the a posteriori solution in Northern China, despite remaining underestimations. In Western Europe and Eastern US, the optimized columns are still lower than OMI (up to 25 %), but in good agreement with SCIAMACHY data, although the MAXLOSS inversion leads to an overestimation of the columns over Europe in summertime. In Southeast Asia, the a priori columns capture quite well the seasonal pattern of the observed columns from OMI and SCIAMACHY, but their magnitudes are strongly different due to the importance of the $NO + HO_2$ sink in the Tropics in the MAXLOSS case. After inversion,

ACPD
13, 7871–7929, 2013

the match between the modelled and OMI columns is excellent, however, a systematic model overprediction persists with respect to SCIAMACHY data. This overestimation, also found over tropical America and tropical Africa, is possibly related to a misrepresentation in the diurnal cycle of natural fluxes and/or OH levels in these regions.

6.2 Aircraft campaign measurements

Modelled NO_2 profile shapes before and after inversion are evaluated against the two Intercontinental Chemical Transport Experiments INTEX-A and INTEX-B. The INTEX-A field mission (Singh et al., 2006) was undertaken between 1 July to 15 August 2004 over North America (http://www-air.larc.nasa.gov/missions/intexna/intexna.htm). The NO_2 profiles obtained in this mission are described in Singh et al. (2007). The INTEX-B two-phase mission (Singh et al., 2009) was conducted in spring 2006 (1 March–15 May) over Mexico area in March and over the Pacific in April and May (http://www.espo.nasa.gov/intex-b/).

Over North America, the a priori NO_2 model profiles are quite similar with slight differences (less than 20 %) in the continental boundary layer. Both inversions succeed in reducing the bias with the observations in summertime. In spring, the MAXLOSS inversion results lead to large overestimations in the boundary layer. In oceanic locations, the changes inferred by the inversions are small in all cases. Although biased high, the MINLOSS profiles lie closer to the measurements, especially over the North Pacific. The assumed strong sink in the MAXLOSS setup leads to significant NO_2 underestimation over all oceanic regions, especially in the mid- and upper troposphere.

6.3 Lifetimes at megacities

Modelled daytime NO_x lifetimes are compared in Fig. 13 with lifetimes derived over megacities by Beirle et al. (2011), using cloud free OMI NO_2 tropospheric columns retrieved using the algorithm version 1.02 (Boersma et al., 2007). The method used by

ACPD
13, 7871–7929, 2013

Beirle et al. (2011) relies on the observed difference in NO_2 distribution according to wind direction.

Seasonally averaged daytime lifetimes for seven megacities are compared with respective modelled lifetimes averaged between 09:00–13:30 LT from the MINLOSS and MAXLOSS inversions. Two ways for calculating the lifetimes are tested. In the first, organic nitrate and peroxy acyl nitrate formation and export are not considered a NO_x sink for the corresponding grid cell. This method leads to generally longer-than-observed lifetimes, especially in the mid-latitudes during wintertime, when HO_x levels are low. The second method accounts for the net organic nitrate formation rate, and is more appropriate for estimating lifetimes over strong, localized sources, like megacities. The agreement with the observations is markedly improved in this case at most locations, although the model still overpredicts the lifetimes in Moscow and to a lesser extent in Tokyo during winter.

Overall, the seasonality of NO_x lifetimes is surprisingly well captured by both MINLOSS and MAXLOSS inversions. In South China and Singapore the observed lifetimes, ranging between 2 and 4 h, are very well reproduced by both inversions, whereas in Riyadh the lifetimes from MINLOSS are factor of two higher than from MAXLOSS. Although the above analysis lends some confidence to the model results, it appears insufficient to (in)validate either of the two inversion scenarios, given the limitations of a comparison between NO_x lifetimes at different spatial scales.

6.4 Comparison with REASv2 and MEIC emission inventories

Figure 14 compares the annual inversion results from MINLOSS and MAXLOSS with the latest version of the Regional Emission inventory in ASia (REAS version 2) and the Multi-resolution Emission Inventory in China (MEIC) for the year 2007. The a priori inventory used for Asia is REASv1, except for the seasonality which has been calculated as described in Sect. 3.2.

REASv2 was developed recently by updating the REASv1 database, which was a first historical anthropogenic emission inventory in Asia covering the period from 1995

ACPD
13, 7871–7929, 2013

to 2003, whose major emission sources are fuel combustion, industrial process, and agricultural activities. The new REAS inventory includes most of major air pollutants and greenhouse gases: SO_2, NO_x, CO, NMVOC, PM_{10}, $PM_{2.5}$, BC, OC, NH_3, CH_4, N_2O, and CO_2. Target years are from 2000 to 2008 and areas are expanded from East, Southeast and South Asia of REASv1 to Central Asia and Asian part of Russia (Ural, West and East Siberia, and Far East). Emissions are estimated on a monthly basis for each country and region and are allocated to grids at a $0.25^\circ \times 0.25^\circ$ resolution. Both spatial and temporal resolutions are finer than in REASv1. Activity data such as energy consumption and industrial production were obtained from new statistics and database of power plants as point sources are fully updated. Country- and region-specific parameters such as emission factors and removal efficiencies were also updated by surveying recently published literature for Asian emission inventories. As for Japan, South Korea, and Taiwan, inventories of other research works based on detailed activity data and information were used in REASv2 (Kurokawa et al., 2013).

MEIC is based on a dynamic, technology-based methodology to estimate anthropogenic emission fluxes in China beyond 1990 and until the present date. Emissions are estimated for all anthropogenic sources for ten chemical species: SO_2, NO_x, CO, NMVOC, NH_3, CO_2, PM_{10}, $PM_{2.5}$, BC, and OC. Total NMVOC emissions are further speciated into species for five chemical mechanisms: CBIV, CB05, RADM2, SAPRC99, and SAPRC07. MEIC updates and improves upon the inventories developed by the same group (Zhang et al., 2007, 2009; Lei et al., 2011a). The major improvements of MEIC inventory include unit based emission inventory for power plants (Wang et al., 2012) and cement plants (Lei et al., 2011b), updates of recent activity data and emission factors from literature, and an on-line emission process database (http://www.meicmodel.org). Emissions are available for four aggregated sectors, namely, power generation, industry, residential and transportation, with monthly temporal variation and 0.25° spatial resolution.

The REASv2 and MEIC distributions are very similar both geographically and temporally over China. At the resolution of the CTM ($2^\circ \times 2.5^\circ$), REASv2 and MEIC are

ACPD
13, 7871–7929, 2013

highly correlated (r = 0.96). Both optimizations bring the model total emissions closer to REASv2 and MEIC: 5.8 and 6.5 Tg N yr^{-1} in MINLOSS and MAXLOSS, vs. 7.2 and 7.6 Tg N yr^{-1} in REASv2 and MEIC, respectively. In terms of seasonal variation (Fig. 8), both optimizations increase the share of summertime emissions compared to the a priori, while reducing the January–March normalized emissions, in better agreement with the bottom-up estimates. Although MINLOSS achieved the best match with the seasonality of Zhang et al. (2007), the seasonality of MAXLOSS emissions is in remarkably good agreement with the more recent inventories, as quantified by the reduced root mean square deviations between MAXLOSS and MEIC (0.14) or REASv2 (0.17), compared to the a priori (0.22). The a priori seasonality (too high in late winter, and too low in summer) is therefore not supported by the satellite observations.

Regarding the spatial distributions of the emissions (Fig. 14), the MINLOSS inversion leads to large emission enhancement in the North China Plain, and to emission decreases in most other regions, leading to a deterioration of the correlation with the MEIC and REASv2 inventories (Table 3). The MAXLOSS inversion realizes a better match with the recent inventories, as seen by the reduced root mean square deviations shown in Table 3.

7 Conclusions

We have investigated the influence of major uncertainties in NO_x chemical sinks on the NO_x columns simulated with the IMAGESv2 model and on the top-down NO_x emission strengths derived by inverse modelling. Uncertainties in four key processes were addressed, namely, (i) the rate of the reaction $NO_2 + OH \rightarrow HNO_3$, (ii) the formation of HNO_3 in the reaction of $NO + HO_2$ as proposed by Butkovskaya et al. (2007, 2009), (iii) the N_2O_5 uptake coefficient on aerosol, and (iv) the regeneration of OH radicals in isoprene oxidation. Through sensitivity model studies, we have shown that these uncertainties imply significant differences in the predicted NO_x columns and lifetimes:

ACPD
13, 7871–7929, 2013

1. Including the reaction $NO + HO_2 \rightarrow HNO_3$ in the model leads to NO_x column decreases estimated at ca. 60 % in oceanic regions and at 30 % over the continental Tropics, whereas the tropospheric NO_x lifetime is reduced globally by 35 %.

2. The use of laboratory-based rates for the uptake of N_2O_5 by aerosols, instead of the low value (0.003) suggested by field data, is found to strongly enhance the total NO_x column sink during winter at mid- and at high lattudes, by about a factor of two, whereas the global NO_x lifetime is decreased by about 6 %. However, this large uncertainty is of little consequence for the comparison of model columns with satellite data obtained around midday local time.

3. The model sensitivity to the rate constant of the $NO_2 + OH$ reaction is found to be relatively weak. Compared to a simulation which uses a rate expression constrained by field data (Henderson et al., 2012), the use of the JPL recommendation (Sander et al., 2011) results in a global decrease of NO_x lifetime by 12 %. Furthermore, the influence of OH recycling in isoprene oxidation is found to be small on the global scale, although it leads to increased (by up to 20 %) loss rates in forested regions.

The consequences of those sink uncertainties on top-down emissions are explored through emission inversion using model settings which either minimize (MINLOSS) or maximize (MAXLOSS) the total sink. Top-down flux estimates for 2007 are obtained from OMI DOMINO v2 NO_2 columns using the IMAGESv2 model and its adjoint.

Major differences are inferred in the NO_x sources derived in both inversions, by virtue of their substantial differences in NO_x loss rates. More specifically, the global NO_x flux from the MAXLOSS inversion is by 50 % higher than in MINLOSS. Interestingly, the largest discrepancies are deduced from soil NO and lightning fluxes (up to a factor of two) reflecting the large sink uncertainties in tropical regions. The global anthropogenic source exhibits weaker differences between the two inversions, and is estimated at 27 and 36 $Tg\,N\,yr^{-1}$ in MINLOSS and MAXLOSS, respectively.

ACPD
13, 7871–7929, 2013

The source was found to be consistently higher in China (5.8–6.5 Tg N yr^{-1}) than in the a priori in both optimizations, and the OMI-derived emission seasonality is found to agree with the recent anthropogenic inventories REASv2 and MEIC. Between the two inversions, MAXLOSS realizes the best match with these two inventories, both in terms of total emission (underestimation by 10–14 % in MAXLOSS, by 20–24 % in MINLOSS) and in terms of spatiotemporal correlation (0.90–0.92 for MAXLOSS, 0.85–0.88 for MINLOSS). Over Europe and North America, the choice of the scenario has a large impact on the top-down flux estimates, and results in either lower or higher emissions than in the a priori. Comparisons with INTEX-A and INTEX-B aircraft measurements indicate that the MINLOSS scenario provides the best match with observations both over continents and over ocean, thereby comforting the $NO_2 + OH$ rate expression recommended by Henderson et al. (2012), which was also based on INTEX-A data analysis.

Since neither optimization scenario succeeds in improving the agreement with all independent datasets, narrowing down the uncertainties on the rates appears premature based on these results. Whereas comparisons with aircraft measurements and SCIAMACHY data point to MINLOSS as the most likely scenario, an opposite conclusion could be drawn from our analysis of top-down emissions inferred over China. Reasons for this apparent contradiction might be multiple. Other, potentially significant, error sources not considered here may bring additional uncertainties. For instance, organic nitrate formation was shown to dominate the instantaneous NO_x sink in most rural environments (Browne and Cohen, 2012). Of particular relevance, models still strongly underestimate the OH radical levels in large Chinese cities during summer (Hofzumahaus et al., 2009; Lu et al., 2013), possibly pointing to still unknown mechanisms in NMVOC oxidation. HONO emissions and/or heterogeneous formation from NO_x could also contribute to increase OH levels in polluted areas in summer as well as in winter.

In conclusion, the substantial influence of NO_x sink uncertainties on the satellite-derived fluxes shown by our study raises an important issue, generally overlooked in previous inversion studies. Clearly, more research is needed to constrain the relevant processes which might affect NO_x removal. Among these processes, the nitric acid

ACPD
13, 7871–7929, 2013

forming channel in $NO + HO_2$ was found to represent the largest source of uncertainty. In view of its potential importance, confirmation by further laboratory experiments is urgently needed.

Acknowledgement. This research was supported by the Belgian Science Policy Office through the SECPEA and A3C PRODEX projects.

References

Alongi, K. S., Dibble, T. S., Shields, G. C., and Kirschner, K. N.: Exploration of the potential energy surfaces, prediction of atmospheric concentrations, and prediction of vibrational spectra for the $HO_2{\cdot}(H_2O)_n$ (n = 1–2) hydrogen bonded complexes, J. Phys. Chem. A, 110, 3686–3691, 2006. 7878

Atkinson, R., Baulch, D. L., Cox, R. A., Crowley, J. N., Hampson, R. F., Hynes, R. G., Jenkin, M. E., Rossi, M. J., and Troe, J.: Evaluated kinetic and photochemical data for atmospheric chemistry: Volume I – gas phase reactions of O_x, HO_x, NO_x and SO_x species, Atmos. Chem. Phys., 4, 1461–1738, doi:10.5194/acp-4-1461-2004, 2004. 7876

Beaver, M. R., Clair, J. M. St., Paulot, F., Spencer, K. M., Crounse, J. D., LaFranchi, B. W., Min, K. E., Pusede, S. E., Wooldridge, P. J., Schade, G. W., Park, C., Cohen, R. C., and Wennberg, P. O.: Importance of biogenic precursors to the budget of organic nitrates: observations of multifunctional organic nitrates by CIMS and TD-LIF during BEARPEX 2009, Atmos. Chem. Phys., 12, 5773–5785, doi:10.5194/acp-12-5773-2012, 2012. 7880

Beirle, S., Huntrieser, H., and Wagner, T.: Direct satellite observation of lightning-produced NO_x, Atmos. Chem. Phys., 10, 10965–10986, doi:10.5194/acp-10-10965-2010, 2010. 7892

Beirle, S., Boersma, K. F., Platt, U., Lawrence, M. G., and Wagner, T.: Megacity emissions and lifetimes of nitrogen oxides probed from space, Science, 333, 1737, doi:10.1126/science.1207824, 2011. 7896, 7897, 7928

Berndt, T.: Formation of carbonyls and hydroperoxyenals (HPALDs) from the OH radical reaction of isoprene for low-NO_x conditions: influence of temperature and water vapour content, J. Atmos. Chem., 69, 253–272, 2012. 7874

Bertram, T. H., Thornton, J. A., Riedel, T. P., Middlebrook, A. M., Bahreini, R., Bates, T. S., Quinn, P. K., and Coffman, D. J.: Direct observations of N_2O_5 reactivity on ambient aerosol particles, Geophys. Res. Lett., 36, L19803, doi:10.1029/2009GL040248, 2009. 7879

Boersma, K. F., Eskes, H. J., and Brinksma, E. J.: Error analysis for tropospheric NO_2 retrieval from space, J. Geophys. Res., 109, D04311, doi:10.1029/2003JD003962, 2004. 7895

Boersma, K. F., Eskes, H. J., Meijer, E. W., and Kelder, H. M.: Estimates of lightning NO_x production from GOME satellite observations, Atmos. Chem. Phys., 5, 2311–2331, doi:10.5194/acp-5-2311-2005, 2005. 7892

Boersma, K. F., Eskes, H. J., Veefkind, J. P., Brinksma, E. J., van der A, R. J., Sneep, M., van den Oord, G. H. J., Levelt, P. F., Stammes, P., Gleason, J. F., and Bucsela, E. J.: Near-real time retrieval of tropospheric NO_2 from OMI, Atmos. Chem. Phys., 7, 2103–2118, doi:10.5194/acp-7-2103-2007, 2007. 7884, 7896

Boersma, K. F., Eskes, H. J., Dirksen, R. J., van der A, R. J., Veefkind, J. P., Stammes, P., Huijnen, V., Kleipool, Q. L., Sneep, M., Claas, J., Leitão, J., Richter, A., Zhou, Y., and Brunner, D.: An improved tropospheric NO_2 column retrieval algorithm for the Ozone Monitoring Instrument, Atmos. Meas. Tech., 4, 1905–1928, doi:10.5194/amt-4-1905-2011, 2011. 7875, 7884

Bond, T. C., Streets, D. G., Yarber, K. F., Nelson, S. M., Woo, J.-H., and Klimont, Z.: A technology-based global inventory of black and organic carbon emissions from combustion, J. Geophys. Res., 109, D14203, doi:10.1029/2003JD003697, 2004. 7886

Brown, S. S., William, P., Dube, W. P., Fuchs, H., Ryerson, T. B., Brock, C. A., Bahreini, R., Middlebrook, A. M., Wollny, A. G., Neuman, J. A., Atlas, E., Roberts, J. M., Osthoff, H. D., Trainer, M., Fehsenfeld, F. C., and Ravishankara, A. R.: Reactive uptake coefficients for N_2O_5 determined from aircraft measurements during the Second Texas Air Quality Study: comparison to current model parameterizations, J. Geophys. Res., 114, D00F10, doi:10.1029/2008JD011679, 2009. 7874, 7879, 7880, 7913

Browne, E. C., Perring, A. E., Wooldridge, P. J., Apel, E., Hall, S. R., Huey, L. G., Mao, J., Spencer, K. M., Clair, J. M. St., Weinheimer, A. J., Wisthaler, A., and Cohen, R. C.: Global and regional effects of the photochemistry of $CH_3O_2NO_2$: evidence from ARCTAS, Atmos. Chem. Phys., 11, 4209–4219, doi:10.5194/acp-11-4209-2011, 2011. 7926

Browne, E. C. and Cohen, R. C.: Effects of biogenic nitrate chemistry on the NO_x lifetime in remote continental regions, Atmos. Chem. Phys., 12, 11917–11932, doi:10.5194/acp-12-11917-2012, 2012. 7880, 7901

Butkovskaya, N. I., Kukui, A., Pouvesle, N., and Le Bras, G.: Formation of nitric acid in the gas-phase $HO_2 + NO$ reaction: effects of temperature and water vapor, J. Phys. Chem. A, 109, 6509–6520, doi:10.1021/jp051534v, 2005. 7877, 7913

ACPD
13, 7871–7929, 2013

Butkovskaya, N. I., Kukui, A., and Le Bras, G.: HNO_3 forming channel of the $HO_2 + NO$ reaction as a function of pressure and temperature in the ranges of 72–600 Torr and 223–323 K, J. Phys. Chem. A, 111, 9047–9053, 2007. 7874, 7877, 7899

Butkovskaya, N., Rayez, M.-T., Rayez, J.-C., Kukui, A., and Le Bras, G.: Water vapor effect on the HNO_3 yield in the $HO_2 + NO$ reaction: experimental and theoretical evidence, J. Phys. Chem. A, 113, 11327–11342, 2009. 7874, 7877, 7889, 7899, 7913

Butler, T. M., Taraborrelli, D., Brühl, C., Fischer, H., Harder, H., Martinez, M., Williams, J., Lawrence, M. G., and Lelieveld, J.: Improved simulation of isoprene oxidation chemistry with the ECHAM5/MESSy chemistry-climate model: lessons from the GABRIEL airborne field campaign, Atmos. Chem. Phys., 8, 4529–4546, doi:10.5194/acp-8-4529-2008, 2008. 7881

Cariolle, D., Evans, M. J., Chipperfield, M. P., Butkovskaya, N., Kukui, A., and Le Bras, G.: Impact of the new HNO_3-forming channel of the $HO_2 + NO$ reaction on tropospheric HNO_3, NO_x, HO_x and ozone, Atmos. Chem. Phys., 8, 4061–4068, doi:10.5194/acp-8-4061-2008, 2008. 7874, 7877, 7888

Cooper, P. L. and Abbatt, J. P. D.: Heterogeneous interactions of OH and HO_2 radicals with surfaces characteristic of atmospheric particulate matter, J. Phys. Chem., 100, 2249–2254, 1996. 7883

Crounse, J. D., Paulot, F., Kjaergaard, H. G., and Wennberg, P. O.: Peroxy radical isomerisation in the oxidation of isoprene, Phys. Chem. Chem. Phys., 13, 13607–13613, 2011. 7874, 7882

Davis, J. M., Bhave, P. V., and Foley, K. M.: Parameterization of N_2O_5 reaction probabilities on the surface of particles containing ammonium, sulfate, and nitrate, Atmos. Chem. Phys., 8, 5295–5311, doi:10.5194/acp-8-5295-2008, 2008. 7874, 7879, 7880, 7888, 7889, 7913

Donahue, N. M.: Atmospheric chemistry: the reaction that wouldn't quit, Nat. Chem., 3, 98–99, doi:10.1038/nchem.941, 2011. 7876

Elshorbany, Y. F., Kurtenbach, R., Wiesen, P., Lissi, E., Rubio, M., Villena, G., Gramsch, E., Rickard, A. R., Pilling, M. J., and Kleffmann, J.: Oxidation capacity of the city air of Santiago, Chile, Atmos. Chem. Phys., 9, 2257–2273, doi:10.5194/acp-9-2257-2009, 2009. 7882

Erb, K.-H., Gaube, V., Krausmann, F., Plutzar, C., Bondeau, A., and Haberl, H.: A comprehensive global 5 min resolution land-use dataset for the year 2000 consistent with national census data, J. Land Use Science, 2, 191–224, doi:10.1080/17474230701622981, 2007. 7886

Evans, M. J. and Jacob, D. J.: Impact of new laboratory studies of N_2O_5 hydrolysis on global model budgets of tropospheric nitrogen oxides, ozone, and OH, Geophys. Res. Lett., 32, L09813, doi:10.1029/2005GL022469, 2005. 7874, 7879, 7880

Giannelli, R. A., Gilmore, J. H., landman, L., Srivastava, S., Beardsley, M., Brzezinski, D., Dolce, G., Koupal, J., Pedelty, J., and Shyu, G.: Sensitivity analysis of MOBILE6.0, EPA Report EPA420-R-02-035, US, Environmental Protection Agency, Washington, DC 20460 USA, 2002. 7885

Henderson, B. H., Pinder, R. W., Crooks, J., Cohen, R. C., Carlton, A. G., Pye, H. O. T., and Vizuete, W.: Combining Bayesian methods and aircraft observations to constrain the $HO^{\cdot}$ + NO_2 reaction rate, Atmos. Chem. Phys., 12, 653–667, doi:10.5194/acp-12-653-2012, 2012. 7873, 7874, 7876, 7877, 7889, 7900, 7901, 7913

Hofzumahaus, A., Rohrer, F., Lu, K., Bohn, B., Brauers, T., Chang, C.-C., Fuchs, H., Holland, F., Kita, K., Kondo, Y., Li, X., Lou, S., Shao, M., Zeng, L., Wahner, A., and Zhang, Y.: Amplified trace gas removal in the troposphere, Science, 324, 1702–1704, 2009. 7874, 7881, 7901

Hudman, R. C., Moore, N. E., Mebust, A. K., Martin, R. V., Russell, A. R., Valin, L. C., and Cohen, R. C.: Steps towards a mechanistic model of global soil nitric oxide emissions: implementation and space based-constraints, Atmos. Chem. Phys., 12, 7779–7795, doi:10.5194/acp-12-7779-2012, 2012. 7891

Irie, H., Boersma, K. F., Kanaya, Y., Takashima, H., Pan, X., and Wang, Z. F.: Quantitative bias estimates for tropospheric NO_2 columns retrieved from SCIAMACHY, OMI, and GOME-2 using a common standard for East Asia, Atmos. Meas. Tech., 5, 2403–2411, doi:10.5194/amt-5-2403-2012, 2012. 7884

Jacob, D. J.: Heterogeneous chemistry and tropospheric ozone, Atmos. Environ., 34, 2131–2159, doi:10.1016/S1352-2310(99)00462-8, 2000. 7883

Jaeglé, L., Steinberger, L., Martin, R. V., and Chance, K.: Global partitioning of NO_x sources using satellite observations: relative roles of fossil fuel combustion, biomass burning and soil emissions, Faraday Discuss., 130, 407–423, 2005. 7873, 7891

Jenkin, M. E., Murrells, T. P., and Passant, N. R.: The temporal dependence of ozone precursor rmissions: estimation and application, AEA Technology, Report No. AEAT/R/ENV/0355 Issue 1, Culham, Oxfordshire, UK, 2000. 7885

Kanno, N., Tonokura, K., Tezaki, A., and Koshi, M.: Water dependence of the HO_2 self reaction: Kinetics of the HO_2-H_2O complex, J. Phys. Chem. A, 109, 3153–3158, 2005. 7878

ACPD
13, 7871–7929, 2013

Kubistin, D., Harder, H., Martinez, M., Rudolf, M., Sander, R., Bozem, H., Eerdekens, G., Fischer, H., Gurk, C., Klüpfel, T., Königstedt, R., Parchatka, U., Schiller, C. L., Stickler, A., Taraborrelli, D., Williams, J., and Lelieveld, J.: Hydroxyl radicals in the tropical troposphere over the Suriname rainforest: comparison of measurements with the box model MECCA, Atmos. Chem. Phys., 10, 9705–9728, doi:10.5194/acp-10-9705-2010, 2010. 7881

Lei, Y., Zhang, Q., He, K. B., and Streets, D. G.: Primary anthropogenic aerosol emission trends for China, 1990–2005, Atmos. Chem. Phys., 11, 931–954, doi:10.5194/acp-11-931-2011, 2011a. 7898

Lei, Y., Zhang, Q., Nielson, C. P., and He, K.: An inventory of primary air pollutants and CO_2 emissions from cement production in China, 1990–2020, Atmos. Environ., 55, 147–154, 2011b. 7898

Lelieveld, J., Butler, T. M., Crowley, J. N., Dillon, T. J., Fischer, H., Ganzeveld, L., Harder, H., Lawrence, M. G., Martinez, M., Taraborrelli, D., and Williams, J.: Atmospheric oxidation capacity sustained by a tropical forest, Nature, 452, 737–740, 2008. 7874, 7881, 7882, 7883, 7913

Levelt, P. F., Hilsenrath, E., Leppelmeier, G. W., van Den Oord, G. H. J., Bhartia, P. K., Tamminen, J., De Haan, J. F., and Veefkind, P.: Science objectives of the ozone monitoring instrument, Geosci. Remote Sens., 44, 1199–1208, doi:10.1109/TGRS.2006.872336, 2006. 7883

Lin, J.-T., McElroy, M. B., and Boersma, K. F.: Constraint of anthropogenic NO_x emissions in China from different sectors: a new methodology using multiple satellite retrievals, Atmos. Chem. Phys., 10, 63–78, doi:10.5194/acp-10-63-2010, 2010. 7873

Lin, J.-T., Liu, Z., Zhang, Q., Liu, H., Mao, J., and Zhuang, G.: Modeling uncertainties for tropospheric nitrogen dioxide columns affecting satellite-based inverse modeling of nitrogen oxides emissions, Atmos. Chem. Phys., 12, 12255–12275, doi:10.5194/acp-12-12255-2012, 2012a. 7875, 7889

Lin, J.-T.: Satellite constraint for emissions of nitrogen oxides from anthropogenic, lightning and soil sources over East China on a high-resolution grid, Atmos. Chem. Phys., 12, 2881–2898, doi:10.5194/acp-12-2881-2012, 2012b. 7873, 7893

Lu, K. D., Hofzumahaus, A., Holland, F., Bohn, B., Brauers, T., Fuchs, H., Hu, M., Häseler, R., Kita, K., Kondo, Y., Li, X., Lou, S. R., Oebel, A., Shao, M., Zeng, L. M., Wahner, A., Zhu, T., Zhang, Y. H., and Rohrer, F.: Missing OH source in a suburban environment near Beijing:

ACPD
13, 7871–7929, 2013

observed and modelled OH and HO_2 concentrations in summer 2006, Atmos. Chem. Phys., 13, 1057–1080, doi:10.5194/acp-13-1057-2013, 2013. 7881, 7901

Ma, J. Z., Beirle, S., Jin, J. L., Shaiganfar, R., Yan, P., and Wagner, T.: Tropospheric NO_2 vertical column densities over Beijing: results of the first three years of ground-based MAX-DOAS measurements (2008–2011) and satellite validation, Atmos. Chem. Phys., 13, 1547–1567, doi:10.5194/acp-13-1547-2013, 2013. 7884

Macintyre, H. L. and Evans, M. J.: Sensitivity of a global model to the uptake of N_2O_5 by tropospheric aerosol, Atmos. Chem. Phys., 10, 7409–7414, doi:10.5194/acp-10-7409-2010, 2010.

Macintyre, H. L. and Evans, M. J.: Parameterisation and impact of aerosol uptake of HO_2 on a global tropospheric model, Atmos. Chem. Phys., 11, 10965–10974, doi:10.5194/acp-11-10965-2011, 2011. 7883, 7889

Martin, R. V., Sauvage, B., Folkins, I., Sioris, C. E., Boone, C., Bernath, P., and Ziemke, J.: Space-based constraints on the production of nitric acid from lightning, J. Geophys. Res., 112, D09309, doi:10.1029/2006JD007831, 2007. 7885, 7892

Matthews, E.: Global vegetation and land use: new high-resolution data bases for climate studies, J. Clim. Appl. Meteor. 22, 474–487, 1983. 7886

McLinden, C. A., Fioletov, V., Boersma, K. F., Krotkov, N., Sioris, C. E., Veefkind, J. P., and Yang, K.: Air quality over the Canadian oil sands: a first assessment using satellite observations, Geophys. Res. Lett., 39, L04804, doi:10.1029/2011GL050273, 2012. 7884

McNeill, V. F., Patterson, J., Wolfe, G. M., and Thornton, J. A.: The effect of varying levels of surfactant on the reactive uptake of N_2O_5 to aqueous aerosol, Atmos. Chem. Phys., 6, 1635–1644, doi:10.5194/acp-6-1635-2006, 2006. 7879

Metzger, S., Dentener, F., Pandis, S., and Lelieveld, J.: Gas/aerosol partitioning, 1, a computationally efficient model, J. Geophys. Res., 107, 4312, doi:10.1029/2001JD001102, 2002. 7886

Mijling, B. and van der A, R. J.: Using daily satellite observations to estimate emissions of short-lived air pollutants on a mesoscopic scale, J. Geophys. Res., 117, D17302, doi:10.1029/2012JD017817, 2012. 7873

Miyazaki, K., Eskes, H. J., and Sudo, K.: Global NO_x emission estimates derived from an assimilation of OMI tropospheric NO_2 columns, Atmos. Chem. Phys., 12, 2263–2288, doi:10.5194/acp-12-2263-2012, 2012a. 7873, 7884, 7886, 7893

ACPD
13, 7871–7929, 2013

Miyazaki, K., H. J. Eskes, K. Sudo, M. Takigawa, M. van Weele, and K. F. Boersma: Simultaneous assimilation of satellite NO_2, O_3, CO, and HNO_3 data for the analysis of tropospheric chemical composition and emissions, Atmos. Chem. Phys., 12, 9545–9579, doi:10.5194/acp-12-9545-2012, 2012b. 7884

Mollner, A. K., Valluvadasan, S., Feng, L., Sprague, M. K., Okumura, M., Milligan, D. B., Bloss, W. J., Sander, S. P., Martien, P. T., Harley, R. A., McCoy, A. B., and Carter, W. P. L.: Rate of gas phase association of hydroxyl radical and nitrogen dioxide, Science, 330, 646–649, doi:10.1126/science.1193030, 2010. 7874, 7876, 7877, 7889, 7913

Müller, J.-F. and Stavrakou, T.: Inversion of CO and NO_x emissions using the adjoint of the IMAGES model, Atmos. Chem. Phys., 5, 1157–1186, doi:10.5194/acp-5-1157-2005, 2005. 7873, 7875, 7884, 7891

Müller, J.-F., Stavrakou, T., Wallens, S., De Smedt, I., Van Roozendael, M., Potosnak, M. J., Rinne, J., Munger, B., Goldstein, A., and Guenther, A. B.: Global isoprene emissions estimated using MEGAN, ECMWF analyses and a detailed canopy environment model, Atmos. Chem. Phys., 8, 1329–1341, doi:10.5194/acp-8-1329-2008, 2008.

Murray, L. T., Jacob, D. J., Logan, J. A., Hudman, R. C., and Koshak, W. J.: Optimized regional and interannual variability of lightning in a global chemical transport model constrained by LIS/OTD satellite data, J. Geophys. Res., J. Geophys. Res., 117, D20307, doi:10.1029/2012JD017934, 2012. 7892

Ohara, T., Akimoto, H., Kurokawa, J., Horii, N., Yamaji, K., Yan, X., and Hayasaka, T.: An Asian emission inventory of anthropogenic emission sources for the period 1980–2020, Atmos. Chem. Phys., 7, 4419–4444, doi:10.5194/acp-7-4419-2007, 2007. 7885

Paulot, F., Henze, D. K., and Wennberg, P. O.: Impact of the isoprene photochemical cascade on tropical ozone, Atmos. Chem. Phys., 12, 1307–1325, doi:10.5194/acp-12-1307-2012, 2012. 7880

Peeters, J. and Müller, J.-F.: HO_x radical regeneration in isoprene oxidation via peroxy radical isomerisations. II: Experimental evidence and global impact, Phys. Chem. Chem. Phys., 12, 14227–14235, doi:10.1039/C0CP00811G, 2010. 7882

Peeters, J., Nguyen, T. L., and Vereecken, L.: HO_x radical regeneration in the oxidation of isoprene, Phys. Chem. Chem. Phys., 11, 5935–5939, doi:10.1039/b908511d, 2009. 7874, 7882

ACPD
13, 7871–7929, 2013

Pickering, K., Wang, Y., Tao, W.-K., Price, C., and Müller, J.-F.: Vertical distributions of lightning NO_x for use in regional and global chemical transport models, J. Geophys. Res., 103, 31203–31216, 1998. 7886

Price, C. and Rind, D.: What determines the cloud-to-ground lightning fraction in thunderstorms? Geophys. Res. Lett., 20, 463–466, 1993. 7885

Ren, X., Olson, J. R., Crawford, J. H., Brune, W. H., Mao, J., Long, R. B., Chen, Z., Chen, G., Avery, M. A., Sachse, G. W., Barrick, J. D., Diskin, G. S., Huey, L. G., Fried, A., Cohen, R. C., Heikes, B., Wennberg, P. O., Singh, H. B., Blake, D. R., and Shetter, R. E.: HO_x chemistry during INTEX-A 2004: observation, model calculation, and comparison with previous studies, J. Geophys. Res., 113, D05310, doi:10.1029/2007JD009166, 2008. 7881

Sander, S. P., Abbatt, J., Barker, J. R., Burkholder, J. B., Friedl, R. R., Golden, D. M., Huie, R. E., Kolb, C. E., Kurylo, M. J., Moortgat, G. K., Orkin, V. L., and Wine, P. H.: Chemical Kinetics and Photochemical Data for Use in Atmospheric Studies, Evaluation number 17, NASA Panel for data evaluation, JPL Publication 10-6, Jet Propulsion Laboratory, Pasadena, available at: http://jpldataeval.jpl.nasa.gov (last access: March 2013), 2011. 7876, 7877, 7900, 7913

Sandu, A. and Sander, R.: Technical note: Simulating chemical systems in Fortran90 and Matlab with the Kinetic PreProcessor KPP-2.1, Atmos. Chem. Phys., 6, 187–195, doi:10.5194/acp-6-187-2006, 2006. 7884

Saunders, S. M., Jenkin, M. E., Derwent, R. G., and Pilling, M. J.: Protocol for the development of the Master Chemical Mechanism, MCM v3 (Part A): tropospheric degradation of non-aromatic volatile organic compounds, Atmos. Chem. Phys., 3, 161–180, doi:10.5194/acp-3-161-2003, 2003.

Schumann, U. and Huntrieser, H.: The global lightning-induced nitrogen oxides source, Atmos. Chem. Phys., 7, 3823–3907, doi:10.5194/acp-7-3823-2007, 2007. 7892

Singh, H. B., Brune, W. H., Crawford, J. H., Jacob, D. J., and Russell, P. B.: Overview of the summer 2004 Intercontinental Chemical Transport Experiment-North America (INTEX-A), J. Geophys. Res., 111, D24S01, doi:10.1029/2006JD007905, 2006. 7896

Singh, H. B., Salas, L., Herlth, D., Kolyer, R., Czech, E., Avery, M., Crawford, J. H., Pierce, R. B., Sachse, G. W., Blake, D. R., Cohen, R. C., Bertram, T. H., Perring, A., Wooldridge, P. J., Dibb, J., Huey, G., Hudman, R. C., Turquety, S., Emmons, L. K., Flocke, F., Tang, Y., Carmichael, G. R., and Horowitz, L. W.: Reactive nitrogen distribution and partitioning in the North American troposphere and lowermost stratosphere, J. Geophys. Res., 112, D12S04, doi:10.1029/2006JD007664, 2007. 7896

ACPD
13, 7871–7929, 2013

Singh, H. B., Brune, W. H., Crawford, J. H., Flocke, F., and Jacob, D. J.: Chemistry and transport of pollution over the Gulf of Mexico and the Pacific: spring 2006 INTEX-B campaign overview and first results, Atmos. Chem. Phys., 9, 2301–2318, doi:10.5194/acp-9-2301-2009, 2009. 7896

Sörgel, M., Regelin, E., Bozem, H., Diesch, J.-M., Drewnick, F., Fischer, H., Harder, H., Held, A., Hosaynali-Beygi, Z., Martinez, M., and Zetzsch, C.: Quantification of the unknown HONO daytime source and its relation to NO_2, Atmos. Chem. Phys., 11, 10433–10447, doi:10.5194/acp-11-10433-2011, 2011. 7882

Søvde, O. A., Hoyle, C. R., Myhre, G., and Isaksen, I. S. A.: The HNO_3 forming branch of the HO_2 + NO reaction: pre-industrial-to-present trends in atmospheric species and radiative forcings, Atmos. Chem. Phys., 11, 8929–8943, doi:10.5194/acp-11-8929-2011, 2011. 7877

Stavrakou, T. and Müller, J.-F.: Grid-based versus big region approach for inverting CO emissions using Measurement of Pollution in the Troposphere (MOPITT) data, J. Geophys. Res., 111, D15304, doi:10.1029/2005JD006896, 2006. 7887

Stavrakou, T., Müller, J.-F., Boersma, K. F., De Smedt, I., and van der A, R. J.: Assessing the distribution and growth rates of NO_x emission sources by inverting a 10-year record of NO_2 satellite columns, Geophys. Res. Lett., 35, L10801, doi:10.1029/2008GL033521, 2008. 7873, 7875, 7884, 7887, 7891, 7892, 7893, 7895

Stavrakou, T., Müller, J.-F., De Smedt, I., Van Roozendael, M., van der Werf, G. R., Giglio, L., and Guenther, A.: Evaluating the performance of pyrogenic and biogenic emission inventories against one decade of space-based formaldehyde columns, Atmos. Chem. Phys., 9, 1037–1060, doi:10.5194/acp-9-1037-2009, 2009a. 7885

Stavrakou, T., Müller, J.-F., De Smedt, I., Van Roozendael, M., van der Werf, G. R., Giglio, L., and Guenther, A.: Global emissions of non-methane hydrocarbons deduced from SCIAMACHY formaldehyde columns through 2003–2006, Atmos. Chem. Phys., 9, 3663–3679, doi:10.5194/acp-9-3663-2009, 2009b.

Stavrakou, T., Müller, J.-F., De Smedt, I., Van Roozendael, M., Kanakidou, M., Vrekoussis, M., Wittrock, F., Richter, A., and Burrows, J. P.: The continental source of glyoxal estimated by the synergistic use of spaceborne measurements and inverse modelling, Atmos. Chem. Phys., 9, 8431–8446, doi:10.5194/acp-9-8431-2009, 2009c. 7886

Stavrakou, T., Peeters, J., and Müller, J.-F.: Improved global modelling of HO_x recycling in isoprene oxidation: evaluation against the GABRIEL and INTEX-A aircraft campaign measurements, Atmos. Chem. Phys., 10, 9863–9878, doi:10.5194/acp-10-9863-2010, 2010. 7882

Stavrakou, T., Müller, J.-F., Peeters, J., Razavi, A., Clarisse, L., Clerbaux, C., Coheur, P.-F., Hurtmans, D., De Mazière, M., Vigouroux, C., Deutscher, N. M., Griffith, D. W. T., Jones, N., and Paton-Walsh, C.: Satellite evidence for a large source of formic acid from boreal and tropical forests, Nature Geosci., 5, 26–30, doi:10.1038/ngeo1354, 2012. 7875

Steinkamp, J. and Lawrence, M. G.: Improvement and evaluation of simulated global biogenic soil NO emissions in an AC-GCM, Atmos. Chem. Phys., 11, 6063–6082, doi:10.5194/acp-11-6063-2011, 2011. 7886, 7891

Stone, D., Evans, M. J., Edwards, P. M., Commane, R., Ingham, T., Rickard, A. R., Brookes, D. M., Hopkins, J., Leigh, R. J., Lewis, A. C., Monks, P. S., Oram, D., Reeves, C. E., Stewart, D., and Heard, D. E.: Isoprene oxidation mechanisms: measurements and modelling of OH and HO_2 over a South-East Asian tropical rainforest during the OP3 field campaign, Atmos. Chem. Phys., 11, 6749–6771, doi:10.5194/acp-11-6749-2011, 2011. 7881

Su, H., Cheng, Y. F., Shao, M., Gao, D. F., Yu, Z. Y., Zeng, L. M., Slanina, J., Zhang, Y. H., and Wiedensohler, A.: Nitrous acid (HONO) and its daytime sources at a rural site during the 2004 PRIDE-PRD experiment in China, J. Geophys. Res., 113, D14312, doi:10.1029/2007JD009060, 2008. 7882

Su, H., Cheng, Y., Oswald, R., Behrendt, T., Trebs, I., Meixner, F. X., Andreae, M. O., Cheng, P., Zhang, Y., and Pöschl, U.: Soil nitrite as a source of atmospheric HONO and OH radicals, Science, 333, 1616–1618, 2011. 7882

Taketani, F., Kanaya, Y., and Akimoto, H.: Kinetics of heterogeneous reaction of HO_2 radical at ambient concentration levels with $(NH_4)_2SO_4$ and NaCl aerosol particles, J. Phys. Chem. A, 112, 2370–2377, doi:10.1021/jp0769936, 2008. 7883

Taraborrelli, D., Lawrence, M. G., Butler, T. M., Sander, R., and Lelieveld, J.: Mainz Isoprene Mechanism 2 (MIM2): an isoprene oxidation mechanism for regional and global atmospheric modelling, Atmos. Chem. Phys., 9, 2751–2777, doi:10.5194/acp-9-2751-2009, 2009. 7880, 7882

van der Werf, G. R., Randerson, J. T., Giglio, L., Collatz, G. J., Mu, M., Kasibhatla, P. S., Morton, D. C., DeFries, R. S., Jin, Y., and van Leeuwen, T. T.: Global fire emissions and the contribution of deforestation, savanna, forest, agricultural, and peat fires (1997–2009), Atmos. Chem. Phys., 10, 11707–11735, doi:10.5194/acp-10-11707-2010, 2010. 7885, 7886

Wang, S. W., Zhang, Q., Streets, D. G., He, K. B., Martin, R. V., Lamsal, L. N., Chen, D., Lei, Y., and Lu, Z.: Growth in NO_x emissions from power plants in China: bottom-up estimates and

satellite observations, Atmos. Chem. Phys., 12, 4429–4447, doi:10.5194/acp-12-4429-2012, 2012. 7898

Wesely, M. L.: Parameterization of surface resistance to gaseous dry deposition in regional-scale numerical models, Atmos. Environ., 23, 1293–1304, 1989. 7880

Wiedinmyer, C., Akagi, S. K., Yokelson, R. J., Emmons, L. K., Al-Saadi, J. A., Orlando, J. J., and Soja, A. J.: The Fire INventory from NCAR (FINN): a high resolution global model to estimate the emissions from open burning, Geosci. Model Dev., 4, 625–641, doi:10.5194/gmd-4-625-2011, 2011. 7892

Yienger, J. J. and Levy, H.: Empirical model of global soil-biogenic NO_x emissions, J. Geophys. Res., 100, 11447–11464, 1995. 7886, 7891

Zhang, Q., Streets, D. G., He, K., Wang, Y., Richter, A., Burrows, J. P., Uno, I., Jang, C. J., Chen, D., Yao, Z., and Lei, Y.: NO_x emission trends for China, 1995–2004: the view from the ground and the view from space, J. Geophys. Res., 112, D22306, doi:10.1029/2007JD008684, 2007. 7893, 7894, 7898, 7899

Zhang, Q., Streets, D. G., Carmichael, G. R., He, K. B., Huo, H., Kannari, A., Klimont, Z., Park, I. S., Reddy, S., Fu, J. S., Chen, D., Duan, L., Lei, Y., Wang, L. T., and Yao, Z. L.: Asian emissions in 2006 for the NASA INTEX-B mission, Atmos. Chem. Phys., 9, 5131–5153, doi:10.5194/acp-9-5131-2009, 2009. 7898

Zhao, C. and Wang, Y.: Assimilated inversion of NO_x emissions over east Asia using OMI NO_2 column measurements, Geophys. Res. Lett., 36, L06805, doi:10.1029/2008GL037123, 2009. 7873

Zhou, X., Zhang, N., TerAvest, M., Tang, D., Hou, J., Bertman, S., Alaghmand, M., Shepson, P. B., Carroll, M. A., Griffith, S., Dusanter, S., and Stevens, P. S.: Nitric acid photolysis on forest canopy surface as a source for tropospheric nitrous acid, Nature Geosci., 4, 440–443, doi:10.1038/ngeo1164, 2011. 7882

ACPD
13, 7871–7929, 2013

Table 1. Forward simulations conducted with the global model, calculated percentage contributions of each sink process to the global tropospheric sink of NO_x, and global tropospheric NO_x lifetime (days).

Simulations	Description	$NO_2 + OH$ sink (%)	$NO + HO_2$ sink (%)	Aerosol sink (%)	Other sinks (%)	Lifetime (days)
MINLOSS	$NO_2 + OH$ reaction rate from Henderson et al. (2012) HNO_3 channel in $NO + HO_2$ ignored $\gamma_{N_2O_5}$ from Brown et al. (2009) $\gamma_{HO_2} = 0.2$ on sulfates MIM2 isoprene oxidation mechanism	73.7	0	7.8	18.5	1.41
MOLLNER	as MINLOSS, $NO_2 + OH$ rate constant from Mollner et al. (2010)	74.1	0	7.6	18.4	1.33
JPL	as MINLOSS, $NO_2 + OH$ rate constant from Sander et al. (2011)	75.0	0	7.1	17.9	1.24
BUTKO1	as MINLOSS, including HNO_3 channel in $NO + HO_2$ (Butkovskaya et al., 2005)	60.6	14.2	7.3	17.9	1.16
BUTKO2	as BUTKO1, including H_2O-assistance to HNO_3 channel (Butkovskaya et al., 2009)	49.8	26.9	6.5	16.9	1.04
DAVIS	as MINLOSS, N_2O_5 reaction probability on sulfate aerosols from Davis et al. (2008)	67.1	0	15.2	17.6	1.32
MIM2+	as MINLOSS, with the MIM2+ isoprene mechanism (Lelieveld et al., 2008)	74.3	0	7.8	17.8	1.38
HO2L	as MINLOSS, HO_2 reaction probability on sulfate aerosols lowered to $\gamma_{HO_2} = 0.05$	74.0	0	7.6	18.4	1.40
MAXLOSS	$NO_2 + OH$ reaction rate from Sander et al. (2011) HNO_3 channel in $NO + HO_2$ from Butkovskaya et al. (2009) $\gamma_{N_2O_5}$ from Davis et al. (2008) $\gamma_{HO_2} = 0.2$ on sulfates MIM2+ isoprene oxidation mechanism	48.9	23.9	11.8	15.4	0.88

ACPD
13, 7871–7929, 2013

Table 2. A priori and a posteriori annual tropospheric NO_x emissions and sinks ($Tg\,yr^{-1}$) according to the MINLOSS and MAXLOSS scenarios. Global anthropogenic includes emissions from shipping and aircraft.

	MINLOSS		MAXLOSS	
Sources	Prior	Optimized	Prior	Optimized
Anthropogenic	29.8	26.7	29.8	36.2
Asia	11.5	10.7	11.5	14.7
Europe	4.7	3.7	4.7	5.2
N. America	6.0	5.0	6.0	7.2
China	4.8	5.8	4.8	6.5
Fires	4.3	5.0	4.3	7.1
Soil	8.0	8.8	8.0	17.9
Lightning	3.0	3.0	3.0	5.2
Total source	45.1	43.6	45.1	66.5
Sinks				
$NO_2 + OH$	34.6	32.9	23.9	37.3
$NO + HO_2$	0.0	0.0	11.7	14.8
$N_2O_5 + H_2O$ on aerosols	3.7	4.1	5.8	9.6
Other	8.7	8.5	7.5	10.2
Total sink	47.0	45.5	48.9	71.9

ACPD
13, 7871–7929, 2013

Table 3. Spatiotemporal correlations and root mean square deviations, expressed in 10^{10} molec cm^{-2} s^{-1}, of monthly NO_x emissions over China.

Correlation	A priori	MINLOSS	MAXLOSS
REASv2	0.916	0.853	0.902
MEIC	0.914	0.877	0.917
RMSD	**A priori**	**MINLOSS**	**MAXLOSS**
REASv2	8.74	10.57	7.58
MEIC	11.1	10.06	7.75

ACPD
13, 7871–7929, 2013

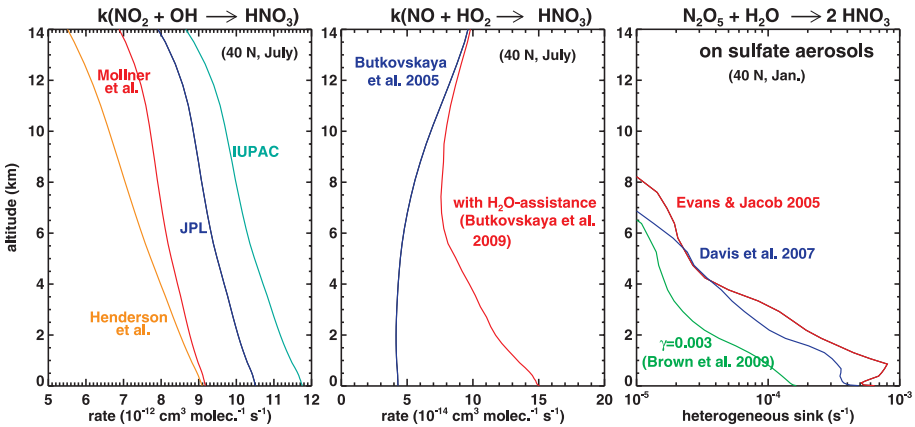

Fig. 1. Zonally averaged at 40° N of the NO_2 + OH reaction rate in July (left), the NO + HO_2 → HNO_3 reaction rate in July (middle), and the heterogeneous sink of N_2O_5 on sulfate aerosols in January (right).

ACPD
13, 7871–7929, 2013

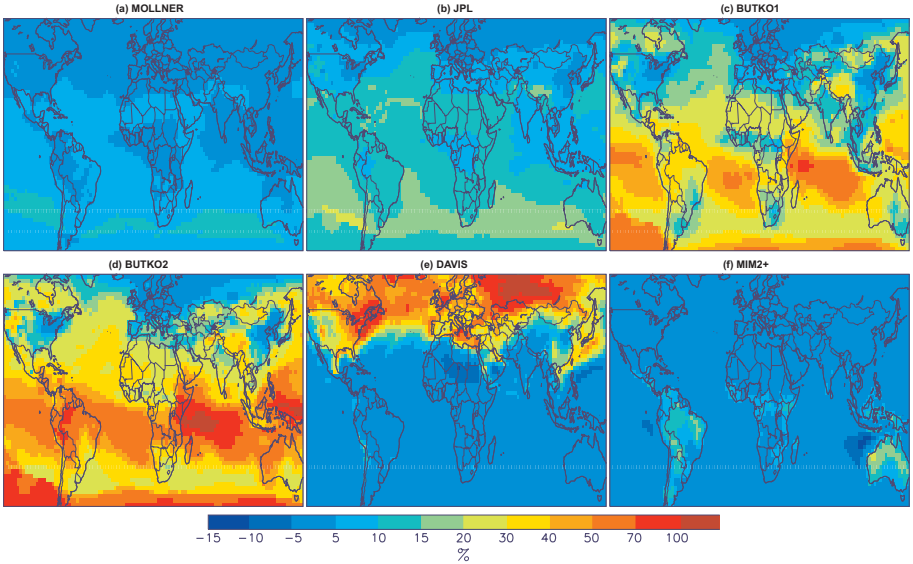

Fig. 2. Percentage difference in the sink rate of the tropospheric NO_x column between the simulations of Table 1 and the base run MINLOSS ((RUN – MINLOSS)/MINLOSS) · 100, for January 2007.

ACPD
13, 7871–7929, 2013

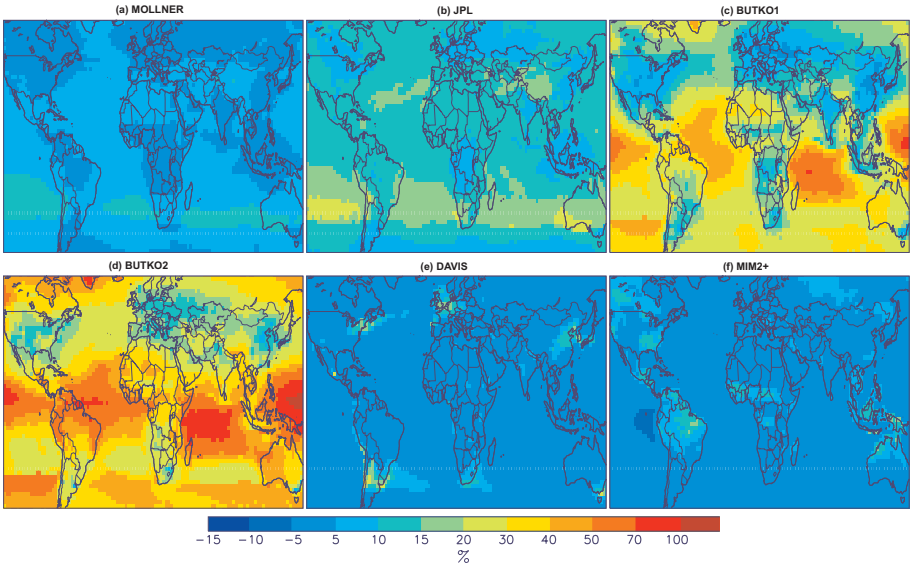

Fig. 3. Same as Fig. 2, for July 2007.

ACPD
13, 7871–7929, 2013

Impact of NO_x sink uncertainties on top-down NO_x emissions

T. Stavrakou et al.

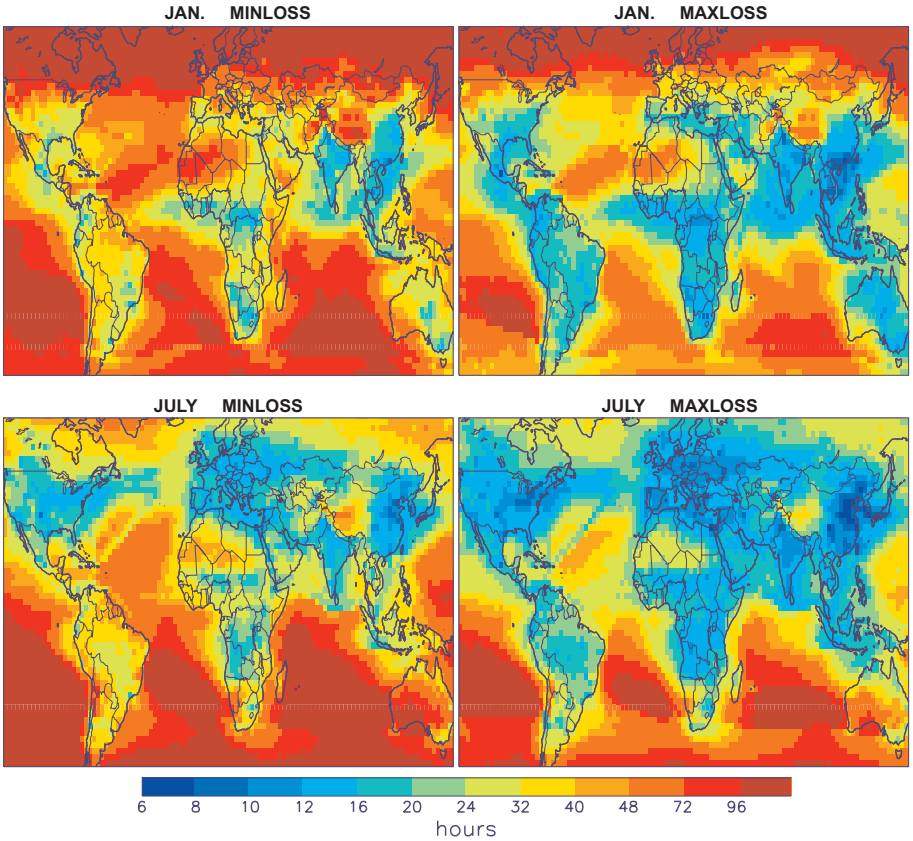

Fig. 4. Comparison of NO_x lifetimes calculated in the MINLOSS and MAXLOSS simulations in January and July 2007.

ACPD
13, 7871–7929, 2013

Impact of NO_x sink uncertainties on top-down NO_x emissions

T. Stavrakou et al.

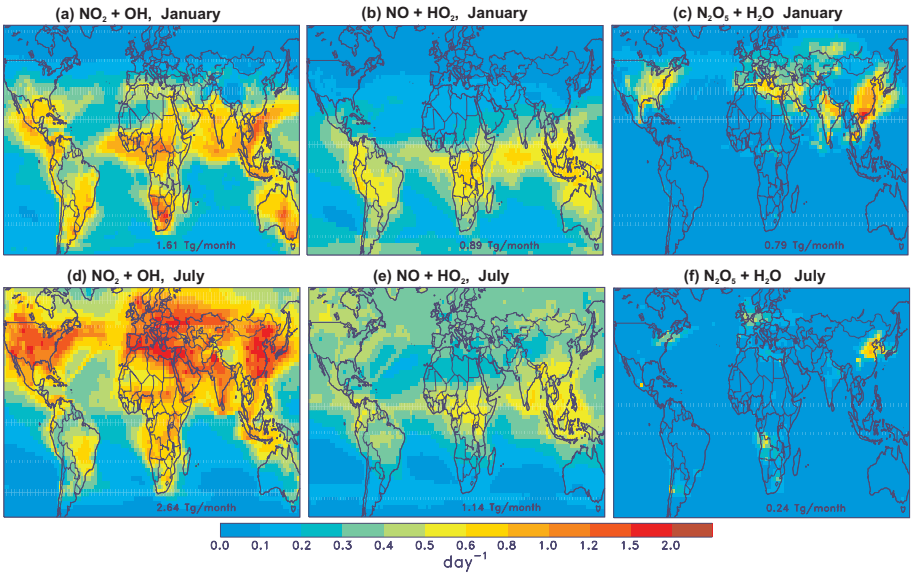

Fig. 5. Calculated contribution of **(a, d)** NO_2 + OH reaction, **(b, e)** the HNO_3-forming channel in NO + HO_2 reaction, and **(c, f)** the heterogeneous N_2O_5 sink to the tropospheric NO_x sink rate (day^{-1}) in January **(a–c)** and July **(d–f)** for the MAXLOSS simulation.

ACPD
13, 7871–7929, 2013

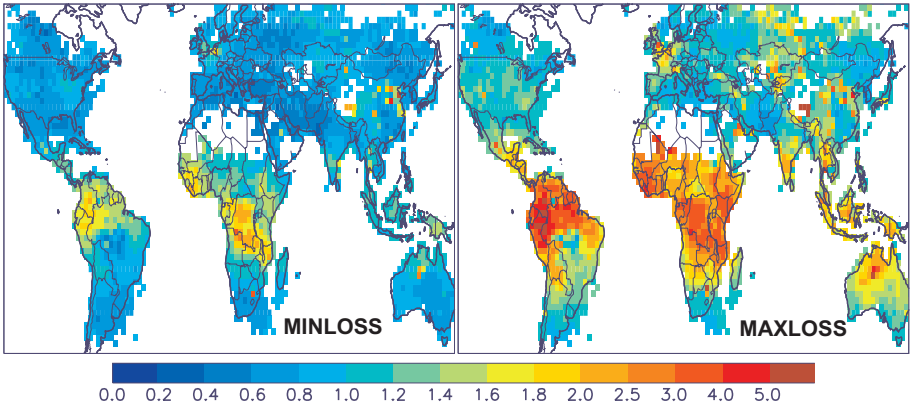

Fig. 6. Annual total NO_x emission update (optimized/a priori) inferred from inversion MINLOSS (left) and MAXLOSS (right).

ACPD
13, 7871–7929, 2013

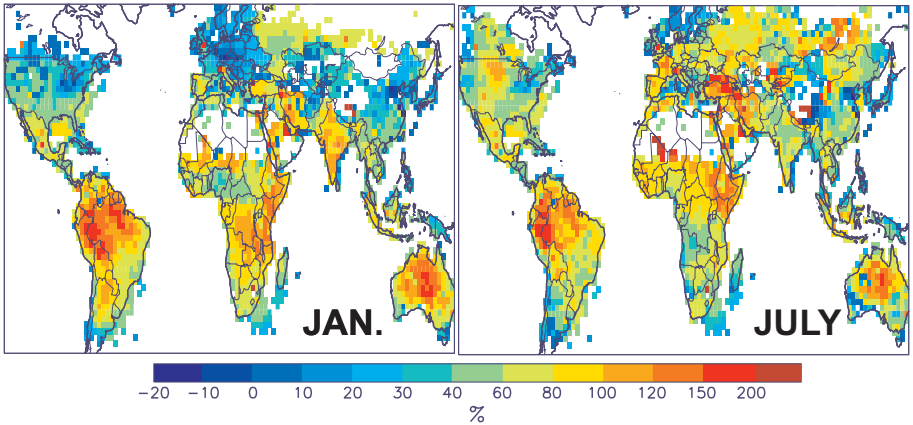

Fig. 7. Percentage difference between inferred total NO_x emission in simulations MINLOSS and MAXLOSS for January and July 2007.

ACPD
13, 7871–7929, 2013

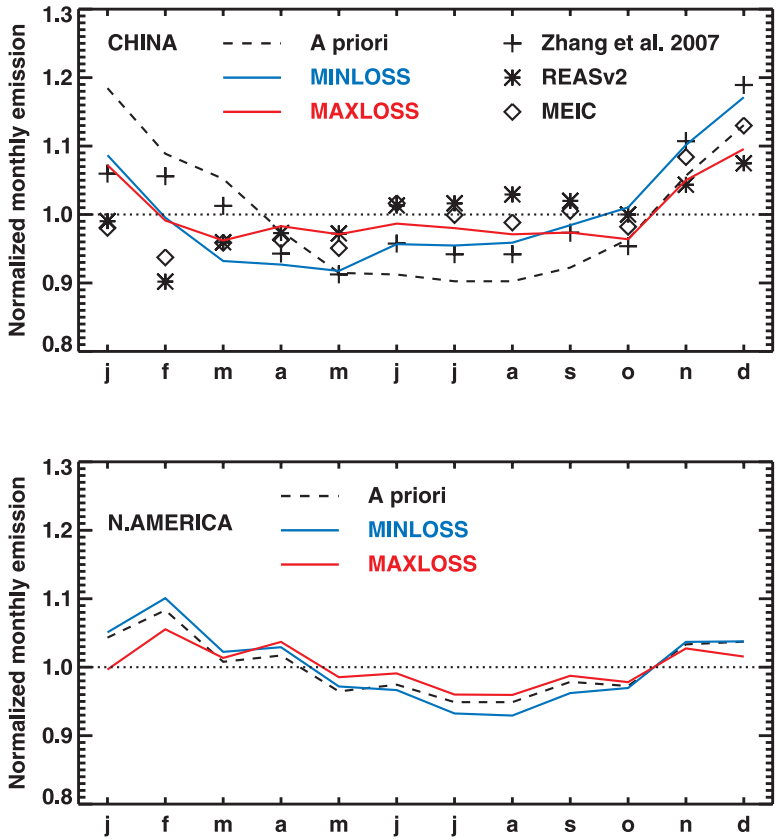

Fig. 8. Normalized seasonal variation of anthropogenic emissions over China (top) and North America (bottom).

ACPD
13, 7871–7929, 2013

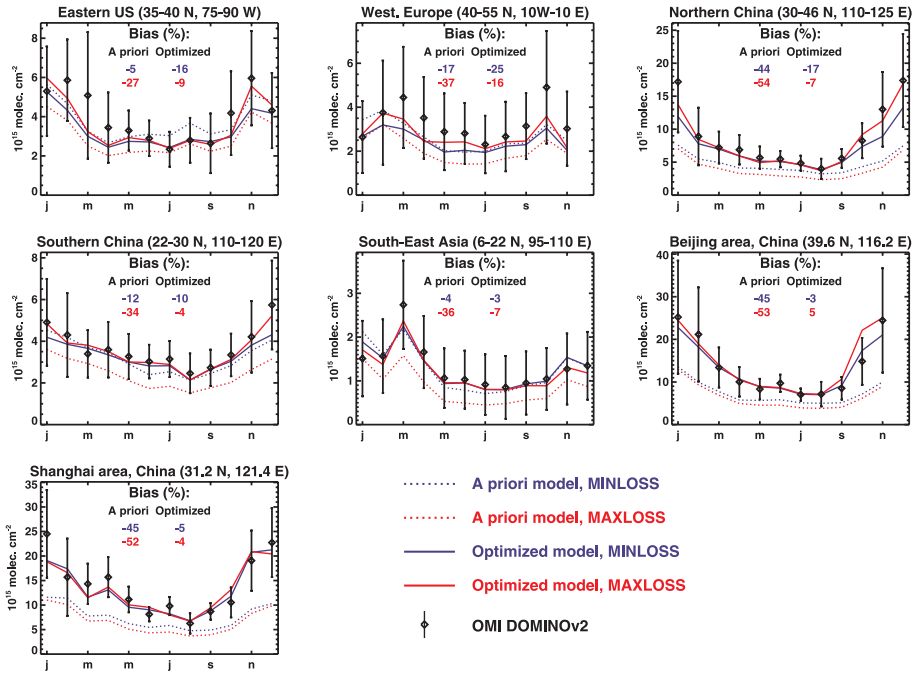

Fig. 9. Seasonal variation of NO_2 columns over large regions. Comparisons between OMI retrievals (diamonds), a priori (dotted), and optimized (solid) columns in MINLOSS (blue) and MAXLOSS (red) for 2007. Percentage biases are given inset. The NO_2 column errors are as described in Sect. 3.2.

ACPD
13, 7871–7929, 2013

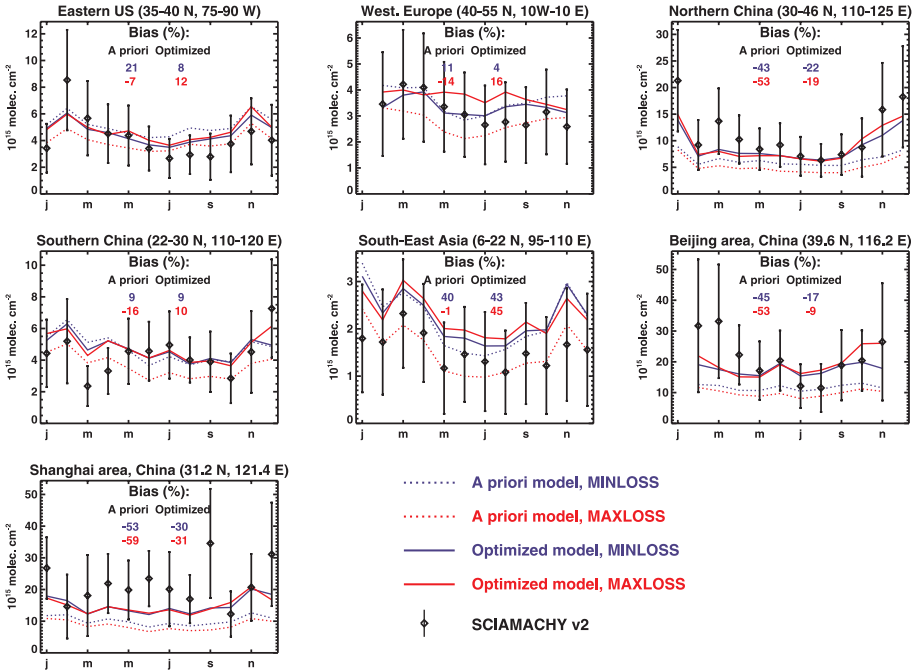

Fig. 10. Same as Fig. 9 but using SCIAMACHYv2 NO_2 retrievals and modelled columns calculated at the SCIAMACHY overpass time (10:00 LT). The NO_2 column errors are as described in Sect. 6.

ACPD
13, 7871–7929, 2013

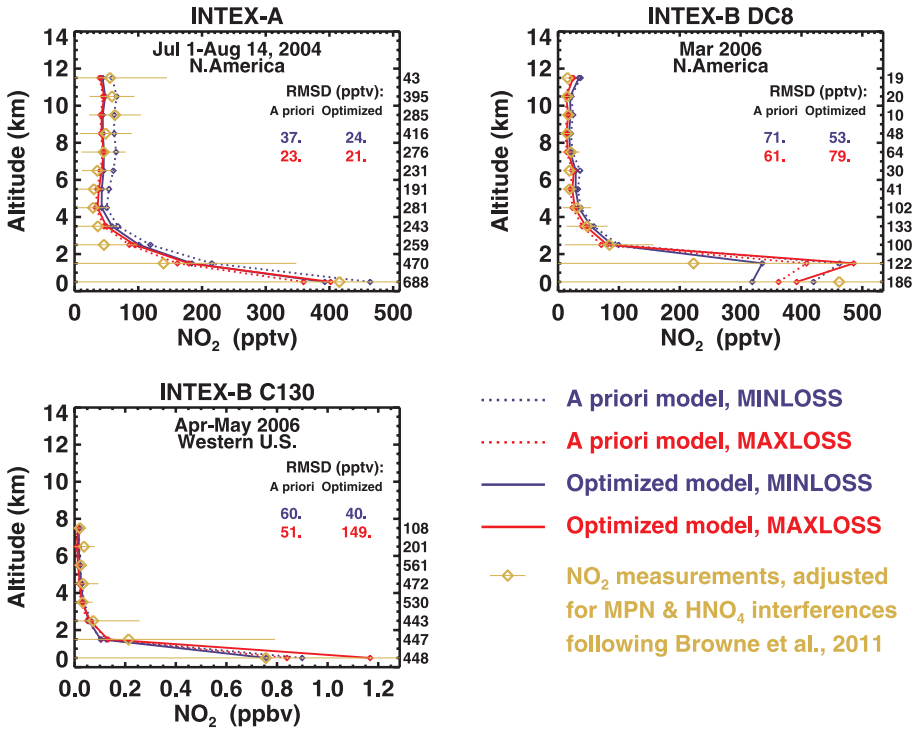

Fig. 11. A priori and optimized modelled NO_2 mixing ratios compared with observed mixing ratios during the INTEX-A and INTEX-B missions over North America. Observed NO_2 mixing ratios are adjusted for methyl peroxy nitrate (MPN) and HNO_4 interferences according to Browne et al. (2011).

ACPD
13, 7871–7929, 2013

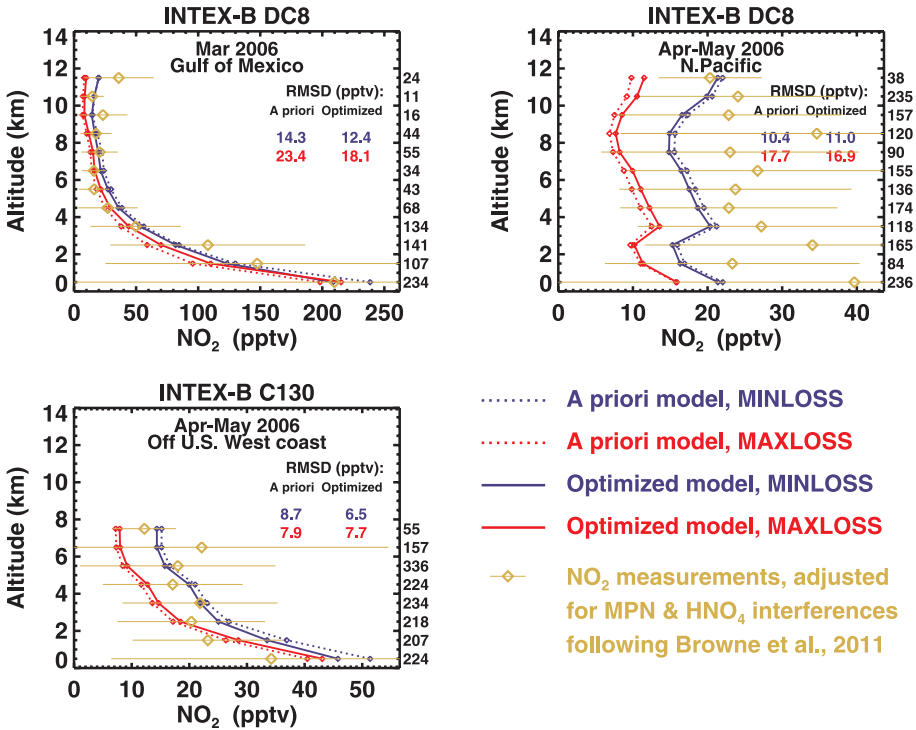

Fig. 12. Same as Fig. 11 but for oceanic areas.

ACPD
13, 7871–7929, 2013

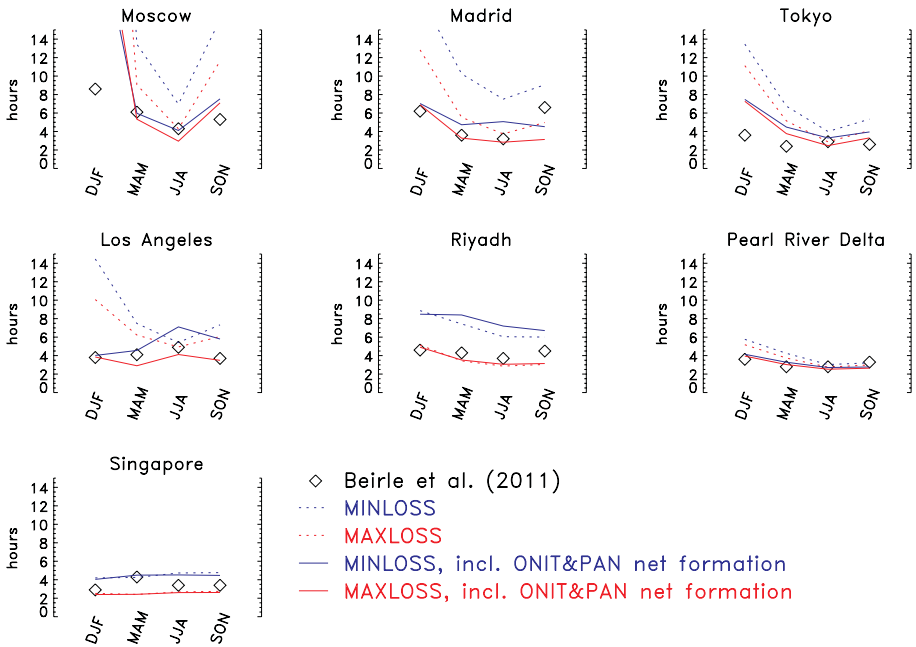

Fig. 13. Comparison between NO_x daytime lifetimes (in black) derived by Beirle et al. (2011) at seven megacities, and modelled lifetimes between 09:00–13:30 LT from the MINLOSS (blue) and MAXLOSS (red) inversions calculated assuming that either nitrate formation and export are not a NO_x sink (dotted lines), or that the net rate of organic nitrate formation should be accounted for (solid lines).

ACPD
13, 7871–7929, 2013

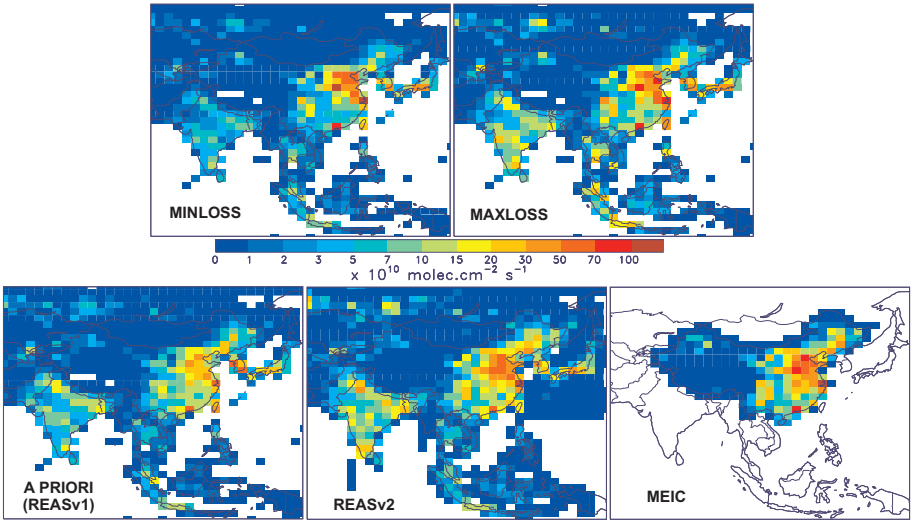

Fig. 14. Comparison between annual anthropogenic emissions inferred from MINLOSS and MAXLOSS inversions (upper panels), and a priori emissions from REASv1, REASv2, and emissions from Multi-Resolution Emission Inventory in China (MEIC) in 2007.

ACPD
13, 7871–7929, 2013